Science Requirements Document
for a
Space Flight Experiment:

Structure and Response of Spherical Diffusion Flames (s-Flame)

January 25, 2010 (SCR version)

Principal Investigator: Chung K. Law, Princeton University
Co-Investigator: Stephen D. Tse, Rutgers University
Co-Investigator: Kurt R. Sacksteder, NASA Glenn Research Center

0.0 EXECUTIVE SUMMARY

Recognizing that most combustion engines and devices operate on the basis of diffusion flames, the proposed program aims to characterize and gain predictive capability of the structure and dynamics of diffusion flames in simple, well-defined flow fields such that the phenomena of interest can be studied without being unduly complicated and compromised by complex and sometimes non-quantifiable flow field effects. The basic flame configuration adopted for the investigation is the spherically symmetric diffusion flame generated by discharging a fuel gas from a porous spherical burner into a quiescent, oxidizing ambience in microgravity. The one-dimensional nature of the system facilitates data acquisition, data reduction, and computational simulation.

The primary goals of the program are two-fold and strongly interdependent. The first objective is to interrogate the fidelity of the chemical kinetic mechanisms and transport sub-models used in the simulation of aerothermochemical phenomena, and consequently identify possible modifications. The second objective is to characterize and gain predictive capability on spherical diffusion flames.

The space flight program consists of two main parts: (1) Mapping and characterization of the movement of spherical diffusion flames subsequent to ignition from a non-steady-state condition and their extinction boundaries due to direct finite-rate chemistry and indirect radiative heat loss. The emphases are on the relative importance of radiative emission and re-absorption, the examination of the adequacy of the detailed chemical kinetics mechanism and transport sub-models used, and the development of flame front instabilities that could modify the extinction boundaries. Results of the study are of relevance to the development of lean-burn engines for improved efficiency and reduced pollutant emissions. (2) Studies of the response of characteristically sooty flames to a non-steady-state initial condition with respect to the aspects given in (1). The studies will include characterizing soot onset as a function of residence time for expanding flames, as well as soot radiation and transport contributions in spreading, extinction, and instability.

The project involves microgravity experimentation, computational simulation, and, where appropriate, theoretical analysis. Interpretation of all phenomena will emphasize the simultaneous and coupled influence of chemistry and transport.

TABLE OF CONTENTS

0.0 EXECUTIVE SUMMARY ii
TABLE OF CONTENTS iii
1.0 INTRODUCTION AND BACKGROUND 1
1.1 Goals and Overview 1
1.2 Scientific Background 2
1.2.1 One-Dimensional Flames for Fundamental Studies 2
1.2.2 Comprehensiveness of Kinetic Mechanisms 3
1.2.3 Dynamics and Extinction of Diffusion Flames 4
1.2.4 Structure and Response of Sooty Flames to a Non-Steady-State Initial Condition 9
1.3 Status of Understanding from Current Investigation 9
1.3.1 Dynamics and Extinction of Diffusion Flames 10
1.3.1.1 Flame Front Motion 10
1.3.1.2 Quasi-Steady Extinction 12
1.3.1.3 Instability and Extinction 14
1.3.2 Structure and Response of Sooty Flames to a Non-Steady-State Initial Condition 16
1.4 Summary 17
1.5 Journal Publications Resulting from Current Investigation 18
2.0 FLIGHT EXPERIMENT 20
2.1 Objectives of the Flight Investigation 20
2.2 Approach 20
2.2.1 Flame Front Motion 21
2.2.2 Dual Quasi-Steady Extinction Limits at Low and High System Damkohler Numbers 21
2.2.3 Flame Front Instabilities in Non-Premixed Flames 22
2.2.4 Dynamics of Characteristically Sooty Flames 22
2.3 Science Data End Products 23
2.4 Anticipated Knowledge and Value to be Gained 25
2.5 Justification for Extended Duration Microgravity Environment 25
2.5.1 Limitations of Terrestrial (1g laboratory) Testing 25
2.5.2 Limitations of Drop Towers and Aircraft 26
2.5.3 Justification for Space-Flight Facility 26
2.6 Mathematical Modeling and Analysis 26
3.0 EXPERIMENT REQUIREMENTS 28
3.1 Requirements Discussion 28
3.1.1 Experiment Configuration Requirements 28
3.1.1.1 Spherical Burner 28
3.1.1.2 Gas Supply 28
3.1.1.3 Burner Gas Delivery 28
3.1.1.4 Ignition 29
3.1.1.5 Ambient Environment 29
3.1.2 Monitoring Measurements Requirements 30
3.1.2.1 Chamber Pressure 30
3.1.2.2 Chamber Oxygen Concentration (Desired) 30
3.1.2.3 Gas Flowrates 30

3.1.2.4 Acceleration 30
3.1.3 Science Diagnostics Requirements 31
3.1.3.1 Optical access 31
3.1.3.2 Color Imaging 31
3.1.3.3 UV Imaging 31
3.1.3.4 Spherical Burner Temperature 32
3.1.3.5 Gas-Phase Temperature Distribution 32
3.1.3.6 Far-Field Temperature Measurement 33
3.1.3.7 Radiant Emission 33
3.1.3.8 Post-Test Gas Composition (Desired) 34
3.2 Operational Sequence 34
3.3 Test Matrix 35
3.4 Test Matrix Summary 36
3.5 Success Criteria 37
3.5.1 Minimal Success 38
3.5.2 Significant Success 38
3.5.3 Complete Success 38
3.6 Post Flight Data Analysis Plan 39
4.0 REFERENCES 42
5.0 APPENDICES 44
5.1 Oxygen Replenishment Considerations 44
5.2 Quasi-Steady Flame Movement 48
5.3 Heat Transfer to Burner Considerations 49
5.4 UV Imaging: Comparison with Experiment and Computation 52
5.5 *g*-Jitter Considerations 55

1.0 INTRODUCTION AND BACKGROUND

1.1 Goals and Overview

The present program is motivated by both practical and fundamental considerations. On the practical side, it is recognized that since most combustion engines and devices operate on the basis of diffusion flame combustion, their performance in terms of power, efficiency, pollutant emissions, and reliability must necessarily be related to the underlying dynamics and chemistry of diffusion flames. On the fundamental side, it has become increasingly clear that combustion has recently evolved from being an empirical science to an exact, predictive science. As such, combustion phenomena that are sufficiently "clean" and well controlled can now be studied with rigor and confidence, leading to the prospect of the ultimate understanding of unit thermochemical processes as well as the quantification of the associated physico-chemical parameters. Examples are the structure, burning rates, extinction states, and stability boundaries of premixed and diffusion flames, the chemical kinetic mechanisms and the associated rate constants of simple hydrocarbon fuels, the various thermal and mass diffusivities, and the radiation properties. The subject program therefore capitalizes on the unique buoyancy-free environment offered by microgravity to acquire diffusion flame data of high fidelity for such fundamental and canonical studies.

The basic flame configuration adopted for the proposed investigation is the spherically symmetric diffusion flame generated by issuing a fuel mixture into a quiescent oxidizing environment. Schematics of the configurations investigated are shown in Fig. 1.1. The flow field, being steady and one-dimensional, is the simplest and "cleanest" known possible, thereby facilitating data taking, analysis, and interpretation. Furthermore, computational simulation of such a flame is correspondingly simpler, while the comparison between experimental and computed results can also be conducted with enhanced fidelity.

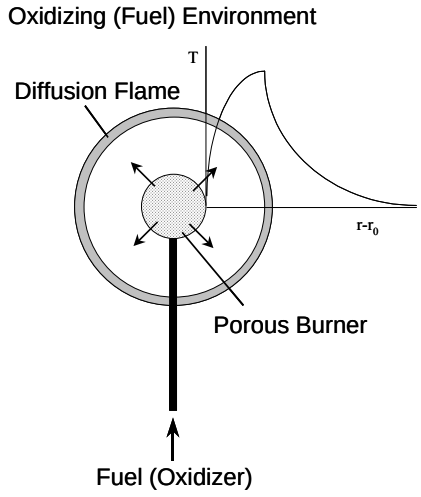

Figure 1.1. Spherical Diffusion Flame Setup. Parentheses ( ) represent inverted configuration.

There are two goals of the present program, which are strongly interdependent. The first goal is to interrogate the fidelity and comprehensiveness of the chemical kinetic mechanisms and transport sub-models used in the simulation of aerothermochemical phenomena, and consequently identify possible modifications. The second goal is to characterize and gain predictive capability on a number of

important unit combustion processes. These include: (1) The dynamics and extinction of diffusion flames, with emphases on fuel vapor accumulation, radiation heat transfer, flame pulsation, and flame kinetics; and (2) the structure and response of sooty flames, with emphases on soot formation and radiative extinction. The interdependence is effected by employing the simple flames of (1) to interrogate and suggest modifications of the kinetic and transport data bases, and then using these data bases to study the chemically and aerodynamically more complex environments of (2) to further scrutinize the comprehensiveness of these data.

In the following we shall first justify the desirability of the flame configuration adopted for the study, then emphasize the need for comprehensiveness in the description of chemical kinetics and transport in combustion studies, and finally discuss the scientific background and merit of the various phenomena to be investigated.

1.2 Scientific Background

1.2.1 One-Dimensional Flames for Fundamental Studies

As noted earlier, studies of fundamental flame properties, and consequently the associated kinetic and transport sub-models and data bases, can be best conducted by using a flame situated in a flow that is the simplest possible. In this way the influence of the flow on the structure of the flame is either minimized or well controlled. Clearly the simplest flow is one that is steady and one-dimensional. For premixed flames such a configuration is realized for a flame stabilized over a porous burner that is planar, cylindrical, or spherical. For diffusion flames, since a steady mathematical solution does not exist for the planar and cylindrical geometries in the doubly infinite or semi-infinite domain, the only possible steady, one-dimensional flame is the spherical flame obtained, for example, by issuing a fuel gas from a porous sphere into a stagnant, unbounded oxidizing environment.

There are three additional observations regarding the issue of one-dimensionality. First, the requirement of spherical symmetry readily implies and thereby justifies the need to perform the experiments in microgravity. Second, while the extensively studied problem of microgravity droplet combustion is spherically symmetric, the phenomenon is inherently not in steady state because the continuously regressing droplet surface can induce unsteady combustion behavior such as those due to fuel vapor accumulation and far-field diffusional unsteadiness.

The last observation is perhaps the most subtle. The structure and response of both premixed and diffusion planar flames have been studied in the counterflow configuration by analyzing variations of flame properties along the axial direction, with the adoption of quasi-one-dimensional or self-similar assumptions. The nonuniformity of the flow is then frequently approximated as a stagnation flow and is characterized by, say, the velocity gradient in the axial direction immediately ahead of the flame. Experimentally, however, the counterflow is usually generated from opposing nozzles and the identification of the proper velocity gradient is somewhat subjective for quantitative studies. Furthermore, there are also physico-chemical processes that are either intrinsically multidimensional or whose presence renders the system non-one-dimensional. For the former we cite radiative transport, whose emission and re-absorption influences on the flame response are now recognized to be crucial, especially for near-limit or sooty flames. For the latter we recognize the misalignment of diffusive and convective transports in the counterflow flame in that diffusion is normal to the flame while convection is along the streamline and hence oblique to the flame. While effects of such a mis-alignment are crucial to the behavior of real flames that are frequently under the influence of aerodynamic straining, the quantitative inaccuracy involved in treating the problem as one-

dimensional has not been assessed. These non-one-dimensional effects are not present in the spherically symmetric configuration because diffusive, convective, and net radiative transports are all in the radial direction. Consequently, interrogation and possible modification of the kinetic and transport inputs can be conducted with greater confidence.

We shall next discuss how the proposed diffusion flame experiments enhance the comprehensiveness of the development of kinetic mechanisms.

1.2.2 Comprehensiveness of Kinetic Mechanisms

Historically, the role of chemistry in the modeling of combustion phenomena has been handled in a rather rudimentary manner. For example, chemical equilibrium was assumed in the analysis of internal combustion engine cycles while infinitely fast chemistry was used in the study of diffusion flames in the flame-sheet limit. In situations where finite-rate chemistry is inherently important, as in the case of premixed flame propagation, the one-step overall Arrhenius-sensitive reaction was frequently used.

Since the late 1970s, however, the fundamental importance of chemical kinetics in combustion phenomena, beyond the one-step description and frequently involving chain mechanisms, has been gradually appreciated. Consequently, at present it is a fairly routine matter to describe laminar flames of simple configurations with detailed chemistry, and to model turbulent flames and engine combustion processes with reduced mechanisms consisting of a few semi-global steps. This heightened awareness of the importance of chemical kinetics has led to a corresponding proliferation in the development of detailed and reduced mechanisms, and in studies in which these mechanisms are incorporated. While this increased activity has led to significant advances in fundamental and practical combustion, there has also been increasing concern over the adequacy of some of the mechanisms proposed, as well as the appropriateness of applying mechanisms beyond their parametric ranges of validity. The controlling issue here is the comprehensiveness of a given mechanism. That is, because of the coupled and nonlinear nature of the chemical reaction rates and pathways with respect to temperature, pressure and species composition, and the extended ranges over which these parameters can vary, a mechanism is considered to be adequate only if it can describe all the possible combustion phenomena and all the chemical responses over the diverse ranges of parametric and system variations that are expected to occur.

There are three major classes of combustion phenomena that a kinetic mechanism, together with diffusive transport sub-models, must be able to describe in order to satisfy comprehensiveness. The first is the homogeneous system, which includes experiments in shock tubes, flow reactors, and perfectly mixed reactors, and the state behind the shock in a detonation wave. The second is the premixed flame whose controlling chemistry can be quite different for lean and rich mixtures. The third is the diffusion flame for which the intrusion of transport on reactions is perhaps the greatest, and the convenience of fuel lean/rich chemistry enjoyed by premixed flames is absent. Thus although chemical effects for diffusion flames are manifested most in the limit situations of ignition and extinction, a satisfactory description could require a greater extent of comprehensiveness than that for either lean or rich premixed flames.

Considerable studies on combustion chemistry have been conducted on homogeneous systems and premixed flames. In particular, extensive research has been recently performed on the computational simulation of simple premixed flames and its subsequent comparison with data obtained from well-controlled experiments. A notable example of the progress is the measurement and prediction of the laminar flame speed, s_L, which is the propagation speed of the hypothetical adiabatic, one-dimensional planar flame in the doubly infinite domain. Up to the seventies, experimental measurements of this important parameter have resulted in values that could differ by factors of two

to three (Andrews and Bradley 1972). It was subsequently recognized (Wu & Law 1985) that such scatters were caused by various forms of aerodynamic stretch such as flow non-uniformity, flame curvature, and flame/flow unsteadiness. Agreement was greatly improved when these stretch effects were systematically removed. Figure 1.2 shows the comparison between recent stretch-compensated experimental data and the computationally simulated values of s_L for hydrogen-air flames at one atmosphere pressure, using currently available detailed chemistry and transport. Results show very good agreement for lean flames, while the flame speeds for rich mixtures are over-predicted. Similar discrepancies also exist for hydrocarbon-air flames. This is not surprising because hydrogen oxidation is one of the building blocks for hydrocarbon oxidation. At present the cause of this discrepancy has been attributed to either insufficiencies in rich hydrogen chemistry or the inaccuracy in the molecular potential parameters used in the computation of the diffusivities of the hydrogen atom.

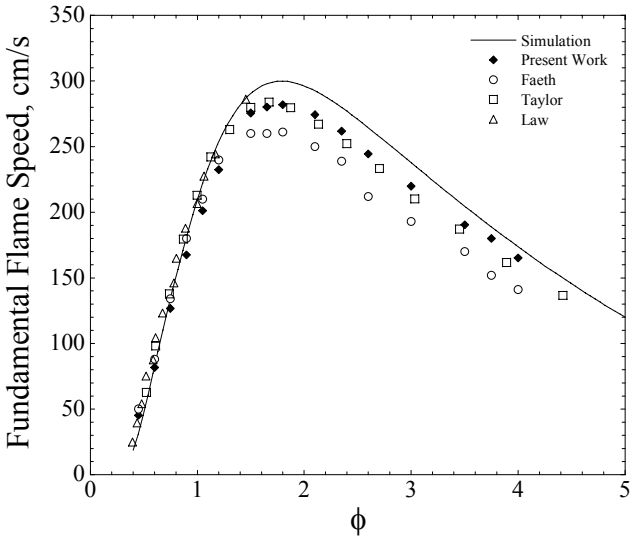

Figure 1.2. Measured and calculated unstretched laminar flame speeds as a function of fuel equivalence ratio for hydrogen/air flames at standard temperature and pressure. Figure from Tse *et al.* (2000).

There has been comparatively less study of flame chemistry by using diffusion flames. Most of these studies have utilized the stagnation flame (e.g., Kent and Williams 1974; Puri & Seshadri 1987; Buipham & Seshadri 1991) and the microgravity droplet flame (e.g., Nagayam et al. 1998; Okai et al. 2000). *The proposed study therefore complements those on homogeneous systems and premixed flames, and completes the triad of combustion phenomena needed for comprehensiveness.*

We shall now separately discuss the scientific background associated with the specific problems that we shall study.

1.2.3 Dynamics and Extinction of Diffusion Flames

The characteristics of diffusion flames can be studied at the "flame-sheet" level of the flame dynamics and the chemistry-affected level of flame extinction. A conveniently identifiable parameter at the flame-sheet level suitable for comparison is perhaps the geometry and location of the flame. A good agreement between experiment and calculation would lend credence to the viability of the basic diffusion flame configuration. As such, the uncertainties and inaccuracies associated with flame

chemistry, including the diffusivity of the hydrogen atom that is only of relevance if we are interested in the flame chemistry, are not present for such diffusion flame sheets.

Furthermore, since the flame location is primarily determined by the state of the stoichiometric transport of fuel and oxidizer, it is not strongly dependent on heat transport and hence the energy conservation equation. Consequently we should expect that comparison between experiment and calculation would be better for diffusion flames than premixed flames. By the same reasoning, if discrepancies still exist, then the cause for the discrepancies observed for the experimental and calculated rich hydrogen-air and hydrocarbon-air premixed flame speeds may not be due to the deficiencies in either the reaction chemistry or the diffusivities.

For the proposed flame experiments, it is anticipated that the initial fuel concentration in the neighborhood of the burner prior to ignition is low. Consequently, upon ignition the flame should be initially located close to the burner surface. It will subsequently move outward to reach the steady-state location, with the concomitant accumulation of fuel vapor in the inner region to the flame (Law *et al*. 1980; King 1996). Thus a stringent test of the predictability of the location of the flame surface can be conducted by tracking the dynamics of the flame surface, allowing for fuel vapor accumulation.

We next discuss the phenomena of flame extinction. While chemical kinetics does not play a role in the limit of the flame-sheet burning of a diffusion flame, it is essential in the description of extinction. Thus the study of extinction provides an alternate means of scrutinizing the flame chemistry, in addition to that offered by premixed flames. From practical considerations extinction is a crucial event in combustion processes and needs to be controlled.

The basic mechanisms governing the extinction of premixed and diffusion flames are somewhat different. Since reaction is basically completed in the reaction zone for most premixed flame phenomena, extinction of a premixed flame is frequently due to loss of the total enthalpy within the flame structure, whether it is thermal or chemical (e.g. reduction in the reactant concentrations due to diffusional stratification) in nature. For diffusion flames, however, the loss is invariably caused by reactant leakage through the reaction zone. Other extinction agents can of course also be present, such as radiative loss or diffusional stratification, but their net effect is manifested in an increase in the amount of reactant leakage. As such, the extinction states for diffusion flames, under apparently different physical situations, can be fundamentally interpreted by the canonical extinction criterion of Linan (1974).

The extinction state is usually represented by the upper turning point of the classical S-shaped ignition and extinction curve. This curve, shown in Fig. 1.3(a), can be obtained by plotting, say, the maximum temperature in the flow field versus the system Damkohler number, *Da*, where *Da* is the ratio of the characteristic flow time to the characteristic chemical time. Figure 1.3(a) shows that, starting from a vigorously burning state on the upper branch, with continuous decrease in *Da* a minimum value can be reached beyond which burning is not possible. This minimum value is then the extinction Damkohler number. In the present experiment, extinction can be brought about for a sufficiently low discharge rate (corresponding to a small characteristic flame size), and hence small residence time (due to the $1/r^2$ characteristic of the velocity flow field), of the fuel stream. Effects of heat loss to the burner can be accounted for by measuring its surface temperature.

In the presence of radiative heat loss, theoretical analyses by Tien (1986), then Chao *et al*. (1991), and Mills and Matalon (1997) have revealed the interesting phenomenon of dual extinction turning points, as schematically shown in Fig. 1.3(b). That is, in addition to the minimum extinction *Da* identified for the purely kinetic limit of burning, there is a maximum extinction *Da* beyond which burning is also not possible. Extinction in this case is caused by the reduction in the flame

temperature due to radiative heat loss which, being a volume process, becomes more severe with increasing size and hence volume of the flame structure. For the present investigation, extinction can be brought about by increasing the flow rate and hence the characteristic flame size. Finite-rate kinetics and hence reactant leakage, of course, is still the route through which the flame is extinguished, as discussed earlier.

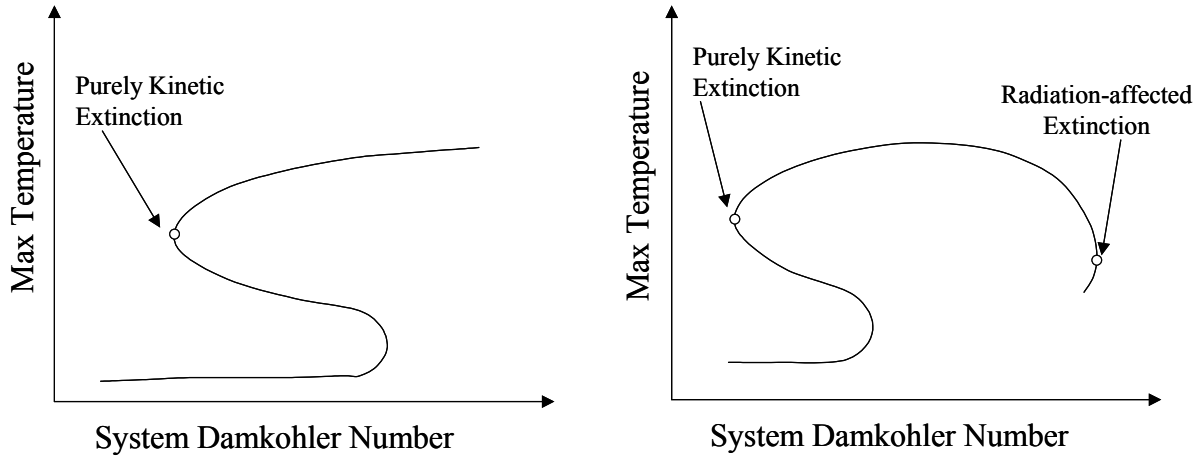

(a) S-curve for purely kinetic extinction **(b)** Dual extinction curve

Figure 1.3. Extinction curves.

To be more specific with this dual extinction phenomenon, let us consider the Damkohler number in the flame region, Da_f, which is the ratio of the characteristic diffusion time to the reaction time at the flame, τ_{Diff}/τ_{Chem}. Since

$$\tau_{Diff} \sim \frac{d_f^2}{\alpha} \quad , \quad \tau_{Chem} \sim \frac{1}{\exp(-T_a/T_f)}, \tag{1}$$

where d_f is the flame diameter, T_f the flame temperature, T_a the activation temperature, and α the thermal diffusivity, we have

$$Da_f \sim d_f^2 \exp(-T_a/T_f), \tag{2}$$

The amount of the radiation loss from the flame is proportional to the flame volume. Since radiation transfer is a temperature-sensitive process, being proportional to T^4, radiative loss is confined to a shell of thickness δ located at d_f, which corresponds to a volume of $4\pi d_f^2 \delta$. This loss then reduces the flame temperature from its adiabatic value, T_{ad}, by an amount

$$(T_{ad} - T_f) \sim d_f^2 \delta, \tag{3}$$

Substituting T_f of the above expression into Da_f, and expanding the exponential function for small values of the loss, we have

$$Da_f \sim d_f^2 \exp(-A d_f^2), \tag{4}$$

where A is a constant. Finally, noting that for the present spherical diffusion flame,

$$m \sim d_f, \tag{5}$$

where m is the mass flow rate (from the porous sphere), we finally have

$$Da_f \sim m^2 \exp(-Am^2)\,. \tag{6}$$

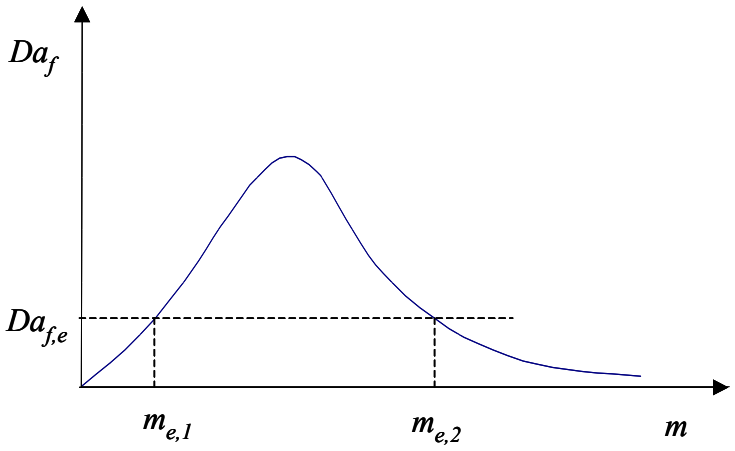

Figure 1.4. Damkohler Number versus mass flow rate.

This final expression, shown in Fig. 1.4 with Da_f plotted versus m, clearly demonstrates the dual extinction nature of the problem. That is, $Da_f \to 0$ as $m \to (0,\infty)$. Thus with extinction occurring at a critical, minimum value, say, $Da_{f,e}$, there exist a low and a high value of the extinction mass flow rate, $m_{e,1}$ and $m_{e,2}$. The lower value corresponds to the m^2 in the coefficient term of Eq. (6), and hence represents purely kinetic extinction, in the absence of heat loss. The upper value corresponds to the m^2 term in the exponent, and hence represents extinction being induced by radiative heat loss.

The final point to note is that since the system Damkohler number Da is defined on the basis of T_{ad}, *without radiative loss*, then $Da \sim m^2$. Consequently, corresponding to $m_{e,1}$ and $m_{e,2}$ we have $Da_{e,1}$ and $Da_{e,2}$, as noted in the theoretical and computational results.

Figure 1.5 computationally confirms the underlying physics shown in Figs. 1.3 and 1.4, presenting the steady-state response curves for a spherical diffusion flame (50%CH_4/50%He fuel stream into 21%O_2/79%He ambient) by plotting the maximum flame temperature as a function of the mass flow rate. Note that the effect of radiative heat loss on the flame response is negligible at low mass flow rates, and the two curves basically overlap and share the same turning point. However, the flame becomes larger in size at larger mass flow rates, and eventually the heat loss due to radiation becomes sufficiently large to extinguish the flame.

This dual extinction phenomenon has been observed in microgravity droplet combustion experiments (Nagayam *et al.*, 1998; Okai *et al.*, 2000). Specifically, for droplets whose initial diameters are fairly large, e.g. between 3 to 5 mm, the extinction droplet diameter was observed to increase with increasing initial droplet diameter, hence supporting the concept of radiative extinction because radiative heat loss increases with increasing volume.

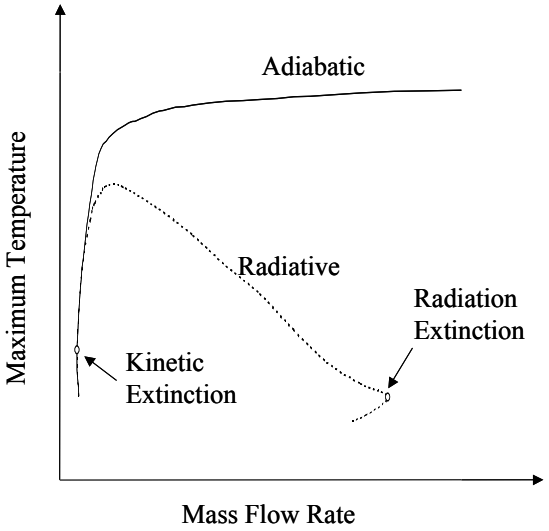

Figure 1.5. Maximum temperature in steady-state spherical methane diffusion flames versus mass flow rate, both adiabatic and with radiative heat loss. Figure adapted from Christiansen et al. (2002).

The proposed porous sphere experiment is expected to complement the droplet experiment in providing additional data on both modes of extinction without the complicating transient effects due to droplet heating and far-field transient diffusion induced by droplet surface regression. The kinetic and radiative effects can therefore be better isolated. Furthermore, for the present experiments, simple gaseous fuels such as methane and ethylene are used instead of the liquid fuels of large molecules such as heptane used in the droplet experiments. The chemical kinetics of the former are substantially simpler and hence better established than the latter. All these factors facilitate the extraction of fundamental kinetic and radiative parameters from the flame data. We note in passing that while methanol and ethanol have also been used in microgravity droplet experiments, water absorption by these droplets during burning can substantially complicate the combustion phenomena, and the subsequent analysis, as the droplet becomes a multicomponent mixture with temporally varying composition.

The above discussions on extinction are based on the premise that the flame burns steadily just prior to the state of extinction. However, asymptotic and simulation studies on premixed flames (Joulin & Clavin 1979; Christiansen *et al.*, 1998) have shown that flames tend to exhibit either cellular or pulsating instabilities just prior to the state of extinction. Furthermore, the tendency to become unstable is aggravated in the presence of heat loss (Joulin & Clavin 1979). Phenomenologically, flame front instability is caused by the disparity between the diffusivities of heat and mass of a gas, represented by its Lewis number *Le* (Sivashinsky 1977, 1983). Cellular flames occur for $Le < 1$ mixtures while pulsating flames occur for $Le >> 1$. Thus the well-established concept that the steady-state turning point corresponds to the state of extinction needs to be revised.

The equivalent phenomenon for spherical diffusion flames was studied theoretically by Cheatham and Matalon (1996). They showed that while the combustion process is absolutely stable at large Damkohler numbers for which the flame is confined to a flame sheet, instability develops for moderate Damkohler numbers and/or oxidizer concentrations. The development is further facilitated with either increasing Lewis number, even in the absence of heat loss, or increasing heat loss, even for unity Le. These results also suggest that, similar to considerations for premixed flames, the

traditional steady-state turning points of the S curve should perhaps also be modified for diffusion flames.

The general phenomena of flame surface dynamics and flame extinction will be experimentally and computationally studied using the present burner-supported spherical diffusion flame. The reactivity and radiative properties of the flame can be varied systematically by changing the fuel ejection rate as well as the sooting tendency of the gaseous fuel. Thus a comparison between the experimental and theoretical extinction flame sizes, with and without substantial radiative heat loss, can be realistically conducted to interrogate/extract the kinetics and quantify the dependence of the dual extinction phenomenon on the extent of radiative heat loss. The presence of flame front instabilities, with the associated cell dimensions and pulsating frequencies, can also be readily observed and quantified.

1.2.4 Structure and Response of Sooty Flames to a Non-Steady-State Initial Condition

It is well established that, for the same flame temperature, soot generation can be more substantial for diffusion flames than for premixed flames. The reason is that, for a diffusion flame, soot is generated on the fuel side of the flame and hence cannot be readily oxidized because the local environment is deficient in oxygen. As such, we study the structure and response of spherical diffusion flames using characteristically sooty fuels. Nonetheless, an important issue in the study of sooty flames is that proper constraints be placed on the system, so that a meaningful comparison can be conducted. Arbitrarily varying fuels/diluents may not lead to meaningful results. A logical constraint is to hold the total energy, and hence to a large extent the maximum flame temperature of the system fixed, as parameters are changed. The second constraint is to hold the flame residence time constant.

We next note that soot is expected to form in a thin layer in the region between the flame and the burner surface, with the exact location determined by the outwardly flowing fuel stream and the inwardly directed thermophoretic force. Consequently, the continuous expansion of the flame front will lead to a corresponding movement of the soot layer. Experimental and computational quantification of such movements can lead to information on the soot formation kinetics as well as the growth of the soot particle size. The presence of soot also provides a radiative heat loss mechanism, and is directly related to our studies on extinction mechanisms, as discussed earlier.

The nonpremixed spherical ethylene flame will serve as the benchmark for the characteristically sooty flame. Ethylene is chosen because of its stronger propensity to form soot than, say, methane. The flame dynamics under microgravity conditions will be specifically examined for the aforementioned soot onset, as a function of the residence time (i.e. characteristic flame size) with no strain and only curvature effects, radiative extinction, and transport induced instability. Since the flame continuously expands due to fuel vapor accumulation, it is expected that soot initiation as well as the subsequent motion of the soot layer will be dynamically evolving as well. Their relative rates of motion should then yield sufficient information for us to assess the intensity of the thermophoretic force experienced by the soot particles. Furthermore, different than the droplet flame, there is no feedback from soot radiation to the droplet, affecting vaporization rate. As a result, soot formation kinetics and flame extinction can be studied at constant mass flow rate.

1.3 Status of Understanding from Current Investigation

Extensive experimental and theoretical progress has been made both in the preparation for the space-based experimentation as well as to obtain new research results in their own right.

Experiments were conducted in the 2.2 s and 5s drop towers of GRC, as well as in a low-buoyancy chamber developed at Princeton. Substantial effort was also expanded towards developing a porous burner which would deliver a radially uniform mass flow at the burner surface. Furthermore, computer codes have been developed for the steady and unsteady solutions of the spherical diffusion flame, with detailed chemistry and transport. The chemical and transport components of these codes will be continuously updated to reflect anticipated advances.

The following is a summary of the major findings of the research performed associated with this program.

1.3.1 Dynamics and Extinction of Diffusion Flames

1.3.1.1 Flame Front Motion

As mentioned previously, upon ignition the flame structure will be localized and situated close to the burner surface. Tracking the subsequent outward movement of the flame front toward its steady-state equilibrium or radiative extinction, and comparing the experimental behavior with computational simulation would allow assessment of the detailed chemistry and transport mechanisms.

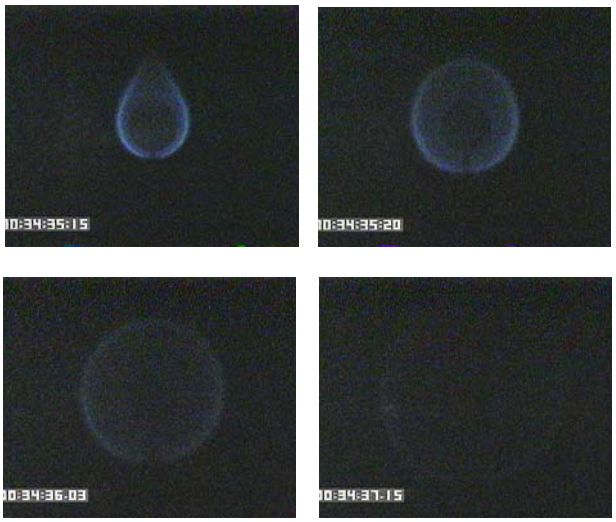

Figure 1.6. Spherical diffusion flame images from 2.2-s drop tower. 50%H_2 / 10%CH_4 / 40%N_2, 8.1mg/s. Figure from Tse *et al*. (2001).

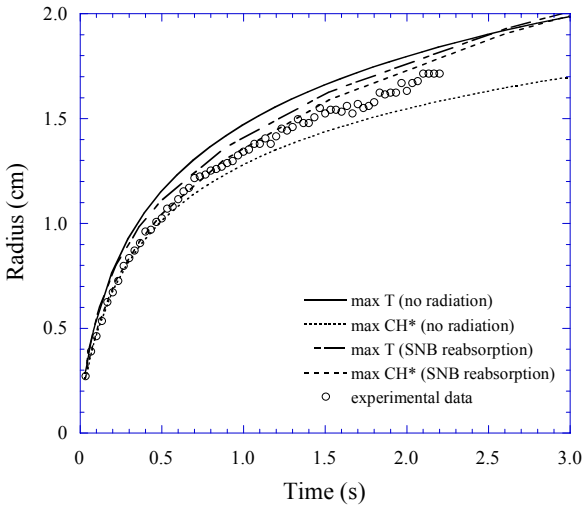

Figure 1.7. Fully transient calculations and experimental data for flame of Fig. 5. Calculated steady-state Max T radius is 4.72cm. Figure from Tse *et al*. (2001).

Experimental data of good quality have been obtained on the transient response of burner-generated spherical diffusion flames in the 2.2-s drop tower facility at the NASA Glenn Research Center. These flames are maintained by constant fuel mass flow rates during an impulsive step from normal-gravity to microgravity conditions. The quality of the spherical diffusion flames produced is excellent, with 0.99 sphericity and 0.94 concentricity (with sphericity and concentricity being respectively defined as the ratio of the horizontal and the vertical diameters of the flame and as the distance between center of the burner and bottom of the flame divided by half of the vertical diameter of the flame), as shown in Fig. 1.6. For the flame evolution process, fully transient calculations with detailed chemistry and transport agree quite satisfactorily with the experimental data (e.g. visible

flame radius) for the flame trajectory, as seen in the representative case of Fig. 1.7, where trajectory simulations with and without radiative effects bound the experimental data corresponding to peak photon emission from the CH* chemiluminescent species (Max [CH*]).

The difference in the separation distance between Max T and Max [CH*] locations can be attributed to effects of heat loss on the flame structure (Fig. 1.8), for the non-radiative and radiative cases. The significantly reduced temperature of the radiative case narrows the flame structure and spatially confines the highly temperature-dependent reaction zone to a thinner region, resulting in the close proximity of Max T and Max [CH*] locations. In other words, the "high" temperature region of the adiabatic flame is much wider than that of the radiative flame, such that peak CH* is closer to Max T for the radiative case. In addition, due to the reduction in maximum temperature, the spatial range with temperature higher than the critical temperature responsible for CH* formation is much narrower in the radiative case.

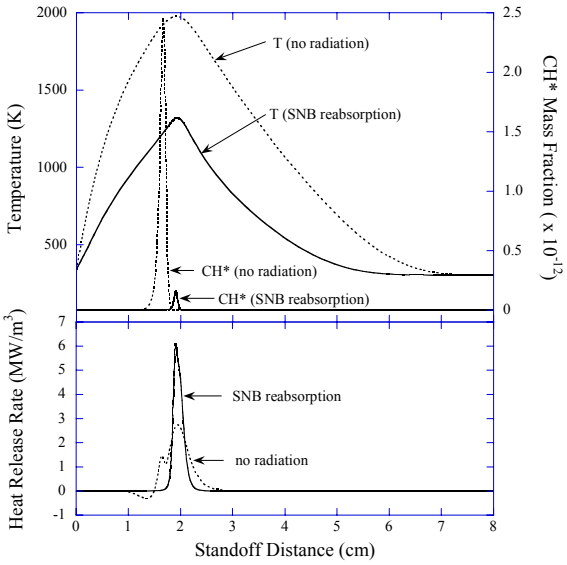

Figure 1.8. Flame structure comparison of non-radiative and SNB optically-thick cases at same time (2.5s) and Max T location, corresponding to Fig. 6. Figure from Tse *et al*. (2001).

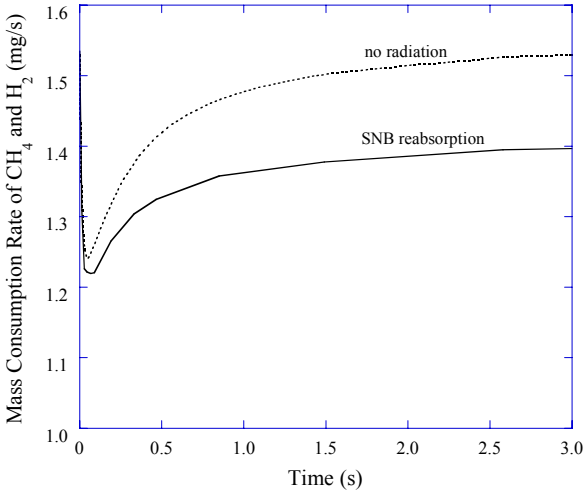

Figure 1.9. Comparison of mass consumption rate for non-radiative and SNB optically-thick cases, corresponding to Fig. 6. Figure from Tse *et al*. (2001).

The slight disparity of the flame trajectories between the non-radiative and radiative cases can be explained in terms of the effects of finite-rate reactions and thermal expansion. As can be seen from Fig. 1.9, due to the reduced reaction rates from reduced temperatures, the mass consumption rate for the radiative case is always smaller than that for the non-radiative case. However, computations reveal that there is very little reactant leakage (until the brief period just preceding flame extinction) for the radiative case despite the smaller mass consumption rate. This phenomenon is readily explained because the flame with radiative loss is able to accumulate more fuel mass for the same volume as compared to the non-radiative case, due to increased gas density from reduced temperature. As a result, during the early stage of flame expansion, the radiative flame is able to maintain a smaller radius with a smaller mass consumption rate and smaller reactant leakage. However, as the flame continues to expand and decrease in temperature, the effect of enhanced mass storage ability cannot compensate for that of decreasing reaction rates, driving the flame to move outwardly faster than in the non-radiative case in order to reduce the fuel mass flux into its consumption zone.

The implications of tracking the flame motion in terms of evaluating chemistry and transport effects are as follows. Since chemilluminescence is directly linked to the detailed chemistry of intermediate species, tracking of the peak temperature position better assesses the transport mechanisms, especially radiative loss/absorption, and consequently the flame structure. Respectively, the tracking of a peak chemiluminescent species, such as OH* and/or CH*, reinforces the validity of the detailed chemistry. Since both chemical kinetics and transport mechanisms are important at extinction, requisite quantitative prediction of extinction phenomena establishes closure.

Experiments have also been performed in low-pressure environments in normal gravity. As suggested and demonstrated by Law et al. (1980) through droplet experiments, problems involving diffusion flame sheets are minimally dependent on the system pressure except for buoyancy effects. Thus by conducting experiments in low pressure and normal gravity, buoyancy effects can be minimized without affecting much the basic features of the flame-sheet problem. Consequently steady-state burner-supported, nearly spherical, diffusion flames have been established and some useful results have been obtained (Yoo et al. 2002). Studies using this approach, however, are limited by small flames and low pressures. Consequently, the experimental flames still suffer a slight degree of asymmetry. Furthermore, the need to work in reduced pressure severely limits the pressure range of investigation for kinetics studies. Since pressure is a sensitive parameter in kinetics, these low-pressure, normal gravity experiments cannot replace normal-pressure, microgravity experiments. We shall return to the topic of the establishment of micro-buoyancy flames in normal gravity in §1.3.1.3.

1.3.1.2 Quasi-Steady Extinction

As inferred from Fig. 1.7, radiative extinction is computationally predicted to occur well beyond the experimental duration of 2.2s. However, for fuel mixtures with relatively low H_2 and high CH_4 concentrations, optically thin computations predict radiative extinction while the experimental flame is still extant and expanding, as shown in Fig. 1.10. As expected, wide-band Planck mean absorption coefficients (T&H), based on Tien (1968) and Hubbard and Tien (1978), over-predict radiative loss compared to the statistical narrow band (SNB) mean coefficients for the optically thin cases. With the treatment of gas-phase self-reabsorption effects, computations utilizing the SNB model seem to better describe the experimental observations in terms of the computational flame surviving beyond the 2.2 seconds.

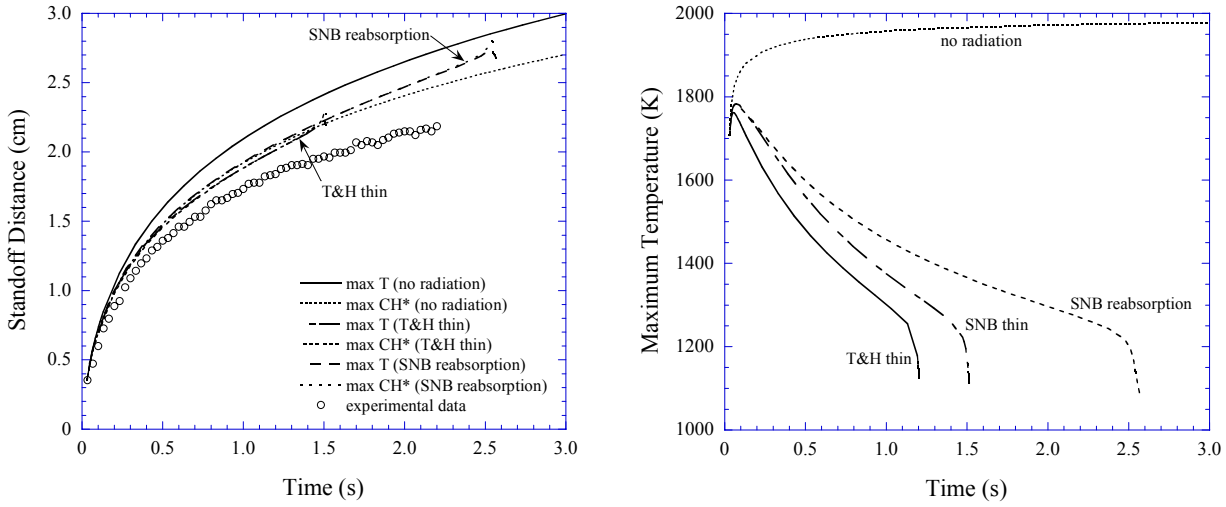

Figure 1.10. Fully transient calculations and experimental data (2.2-s drop-tower) for spherical diffusion flame (20%H2 / 25%CH4 / 55%N2, 15.72mg/s). Figure from Tse *et al.* (2001).

To corroborate the SNB results, aircraft experiments were conducted to extend the microgravity duration. However, radiative extinction was still not observed as predicted from the model, although the experimental g-jitter was sufficiently strong as to preclude a definitive answer. 5-s drop tower experiments showed (Fig. 1.11) an expanding spherical flame which seems to exhibit local extinction (near the top) near the end of the drop. Nonetheless, preliminary 5-s drop tower tests have still been unable to capture the entire flame extinction phenomenon even for the most favorable (minimum flame extinction time, i.e. ~2.5s) case, as shown in Fig. 1.10. Moreover, a large portion of the experimental matrix requires mixtures with longer characteristic extinction times as seen in Fig. 1.12, further stressing the need for longer microgravity duration. The large effect of g-jitter on the experiments and the limited duration of earth-based experiments further substantiate the need for space-based experimentation. Only by resolving such experimental uncertainties and limitations can a computational adjustment of the radiative loss parameters be appropriate.

Figure 1.11. Spherical diffusion flame images from 5.0-s drop tower, showing the onset of radiative extinction. 20%H_2 / 25%CH_4 / 55%N_2, 3mg/s.

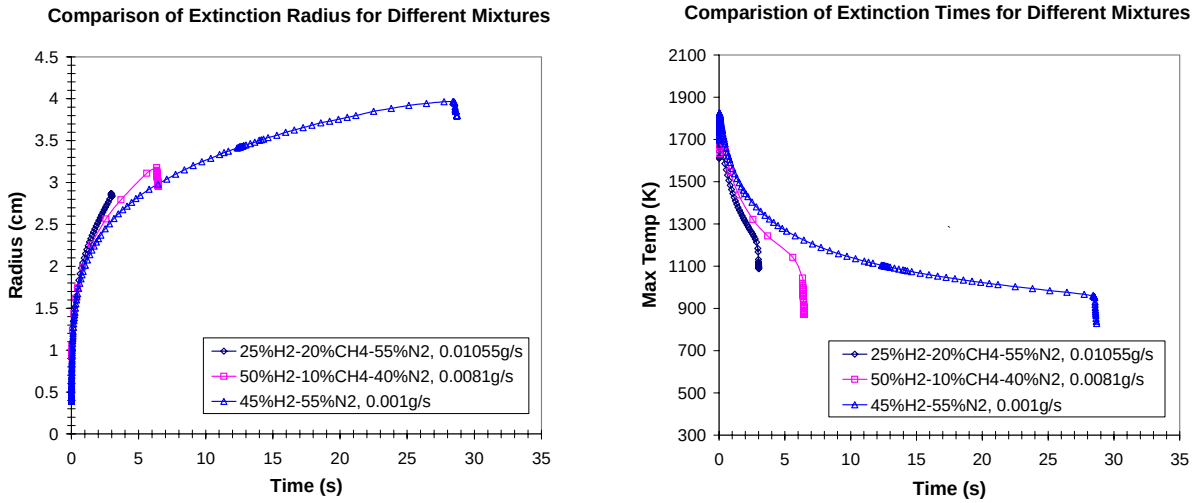

Figure 1.12. Fully transient calculations with SNB model for gas-phase radiative reabsorption for spherical diffusion flame, showing long microgravity duration needed to observe extinction.

It is of critical importance to note that local visible luminosity from the flame provides no indication of either flame strength or flame extinction. In particular, Fig. 1.13 shows that the peak visible emission from CH* decreases rapidly despite an ever increasing flame temperature. The reason for this phenomenon of local visible luminosity decay, as observed in all of the experimental flames, is mainly due to the initially enriched oxygen concentration within the reaction zone of the transient flame structure as compared to the steady-state flame structure. That is, the initial,

"squeezed," flame structure is localized into a thin, high-gradient region, as shown in the temperature profiles of Fig. 1.13. Consequently, the flux of oxidizer into the reaction zone is very large initially, and gradually subsides until it attains its steady-state value. Since the computations reveal that the main CH* production route considered for our flames is through the reaction C_2H+O_2, rather than C_2+OH, increased oxygen concentration available for reaction with C_2H will result in increased chemiluminescence from CH*. The decay of local luminosity of the flame is a consequence of the relaxation of the local CH* luminosity to its steady-state condition from the initial, elevated value. Consequently, experimental investigations of extinction phenomena for such flames should not rely on visible observation, but rather on explicit temperature field measurement (e.g. thin-filament pyrometry, IR radiometer data) in the assessment of the moment of flame extinction.

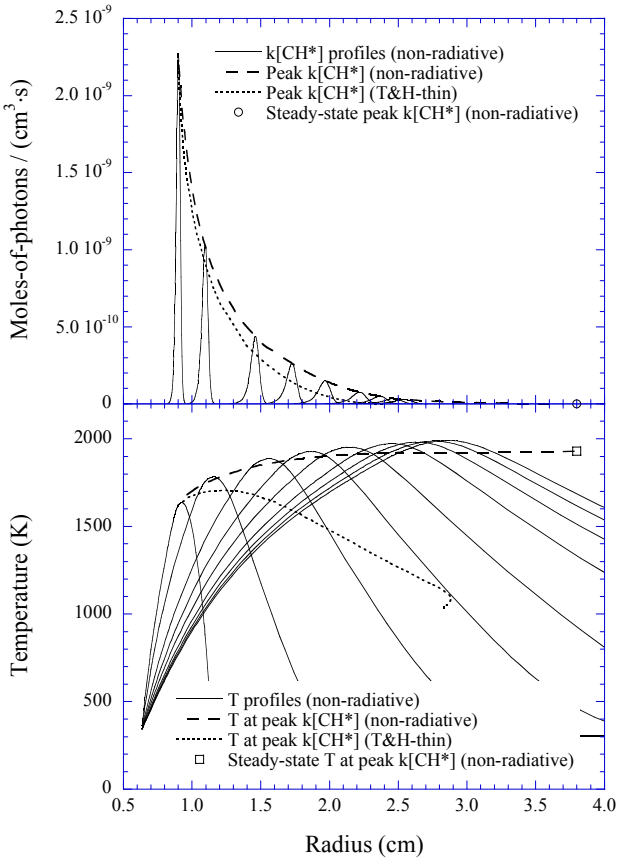

Figure 1.13. Calculated peak CH* chemiluminescence and peak temperature for flame of Fig. 6. Figure from Tse *et al*. (2001).

1.3.1.3 Instability and Extinction

As mentioned in §1.2.1, the preceding discussion should be limited to quasi-steady flames, as determined by satisfying gas-phase steadiness in the reference frame of the moving flame front. The onset of fully transient flame behavior can also lead to extinction as for the case of the 1-D thermal-diffusive pulsating instability. Candle flames in microgravity have displayed flickering instabilities prior to extinction (Dietrich *et al*. 1994). However the geometry of these flames is not optimal for the study and verification of the 1-D pulsating instability, as predicted by theory, because of the potential

influence from the flame holding region which is premixed in nature and hence could conceivably initiate the oscillation. To better understand the mechanism for instability, the transient behavior of spherical diffusion flames was computationally simulated using detailed chemistry and transport (Christiansen *et al*. 2002). Oscillatory instability, as shown in Fig. 1.14, was observed near both the high velocity induced limit (low mass flow rate) and the radiative induced limit (high mass flow rate) of the isola response of flame extinction,. These oscillations typically grow in amplitude until they become large enough to extinguish the flame.

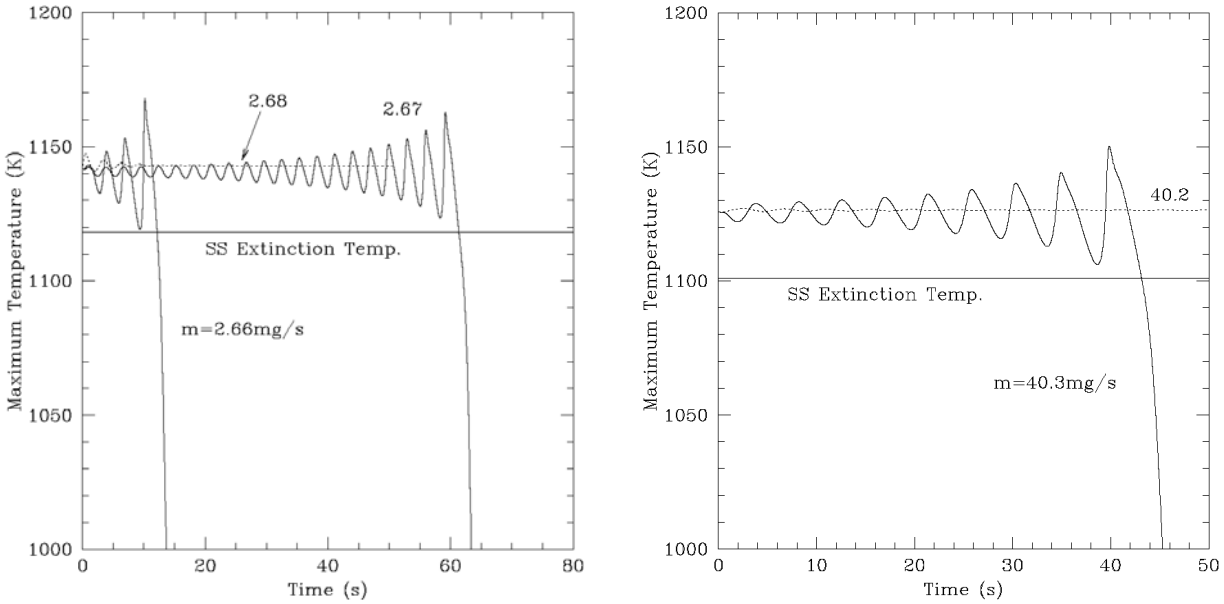

(a) Low mass flow rate limit. **(b)** High mass flow rate limit.

Figure 1.14. Computational simulation of pulsating instability leading to extinction in spherical diffusion flame. 50%CH_4 / 50%He fuel stream into 21%O_2 / 79%He ambient. Figure from Christiansen *et al*. (2002).

Attempts have been made to observe oscillatory instability through low-buoyancy experiments conducted under the influence of normal gravity. The approach is based on the low-pressure droplet experiment of Law and Williams (1973), in which the effect of buoyancy was minimized in a low-pressure environment, typically down to 0.1 atmosphere, beyond which kinetic effects would become severe. Since the present porous sphere is much larger than the droplets, buoyancy is still significant at such a level. In order to further reduce buoyancy, an additional arrangement was implemented (Yoo *et al*. 2002). This involved injecting the oxidizer gas into an environment of low molecular weight fuel such as hydrogen and methane. Buoyancy is reduced because the hot, low-density flame sphere is now situated in an environment of low molecular weight gas. In the experiments various gases (N_2, CO_2, He) were used to change the Lewis number and radiative properties of the gas so that both the transport-induced and reaction-induced limits could be achieved. Extinction was triggered by gradually decreasing the H_2 concentration in the ambient. Results showed that, at the transport-induced limit, extinction is characterized by sudden quenching of the flame, as demonstrated by a rapid decrease of the radiometer signal voltage. However, at the radiation-induced limit, extinction is preceded by oscillations in the flame luminosity that grow in magnitude before extinction, in agreement with the calculation. It is also important to note that both calculation and experiment showed that flame oscillation is characterized by fluctuations in luminosity instead of flame

movement in that the extent of the movement is much smaller than the thickness of the flame. This observation offers interesting implications in flame control.

Studies using this approach, however, are limited for small flames, low pressures, low molecular weight fuels, and the inverse-flame arrangement. Consequently, the extent of investigation is severely limited, and these low-pressure, normal gravity experiments cannot replace normal-pressure, micro-gravity experiments. Additionally, gas-phase radiative loss is significantly smaller at such low pressures, making radiative extinction phenomena difficult to study.

1.3.2 Structure and Response of Sooty Flames to a Non-Steady-State Initial Condition

Initially, partially premixed flames were planned for spaceflight testing. As such, preliminary drop-tower experiments have been conducted for oxygen/propane and oxygen/ethylene mixtures, diluted with argon and nitrogen, issued into air. Varying amounts of oxygen were added to the "fuel" mixture, while keeping the pure fuel mole fraction fixed and altering the relative proportions of inert (i.e. N_2 and Ar) such that the adiabatic flame temperature of the systems were held constant.

The effect of oxygen addition on soot suppression is shown in Fig. 1.15, which presents two cases with the same C_3H_8 fuel concentration, adiabatic flame temperature, and flow rate. The 25%C_3H_8 / 75%Ar mixture produces a sooty flame with yellowish-orange luminescence. By adding O_2 to the mixture and replacing Ar with N_2, a non-sooty flame with only blue luminescence is produced.

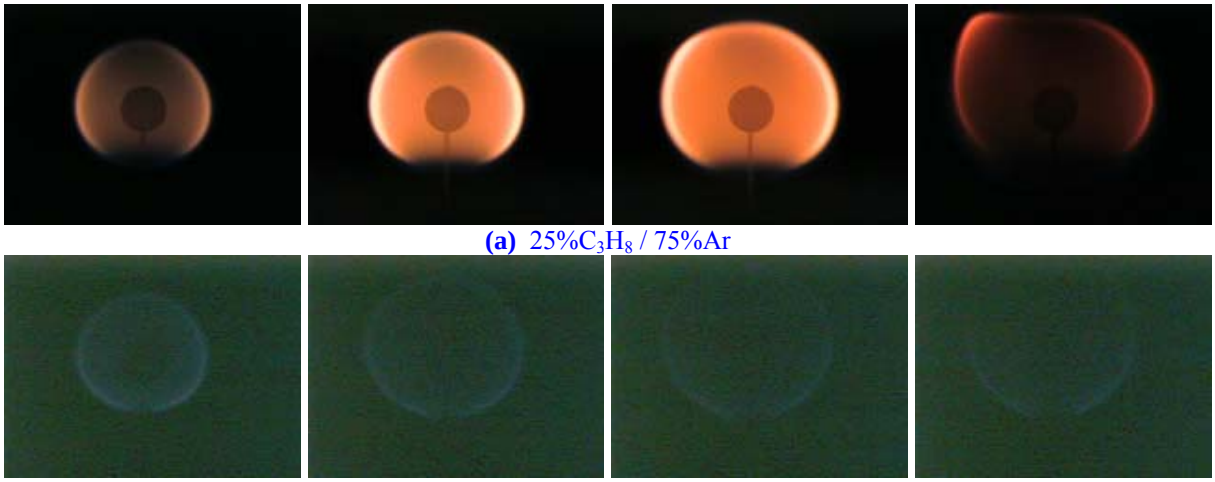

(a) 25%C_3H_8 / 75%Ar

(b) 25%C_3H_8 / 5.8%O_2 / 69.2%N_2

Figure 1.15. Comparison of the effect of partial-premixing on soot formation/suppression for spherical diffusion flames with same fuel concentration, adiabatic flame temperature, and flow rate. Experiments are conducted in the 2.2-s drop tower facility.

The experiments also showed that the formation and suppression of soot in the spherical flame is not only a function of the degree of partial premixing but also of the flow rate. Figure 1.16 shows two cases with the same partially premixed mixture but with different flow rates. It is seen that at the higher flow rate, the flame is sooty with yellowish-orange luminescence, while at the lower flow rate it is almost non-sooty with blue luminescence. This is probably due to reduced residence time for the flame with the lower flow rate. Note the double luminous structure in the lower flow rate flame, showing soot formation within the blue luminescence. The soot luminescence appears to decrease with increasing flame size, similar to the sooty flame of Fig. 1.15. Nonetheless, it is not clear whether this effect is due to soot reduction or only lessened luminescence.

(a) High Flow Rate

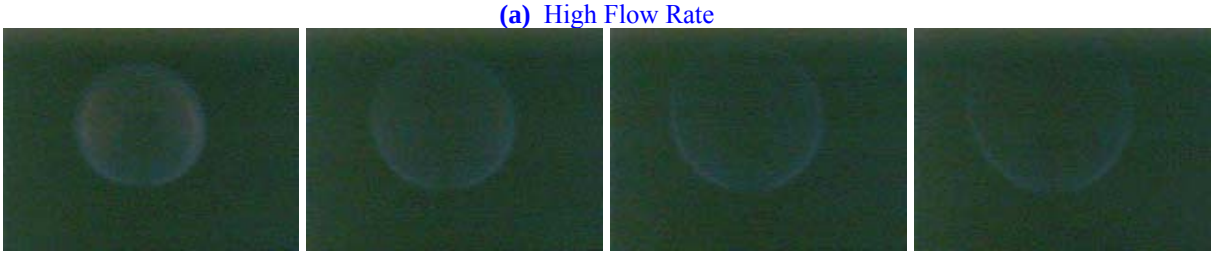

(b) Low Flow Rate

Figure 1.16. Time sequence (increasing from left to right) comparison of the effect of flow rate on soot formation/suppression for partially-premixed spherical diffusion flames. Same mixture for both cases: 25%C_3H_8 / 2%O_2 / 49% Ar / 24% N_2. Experiments are conducted in the 2.2-s drop tower facility.

Although these flames are partially premixed, the effects of fuel concentration, adiabatic flame temperature, and flow rate (residence time) on soot formation/suppression for non-premixed spherical diffusion flames should be similar.

1.4 Summary

Fundamental combustion research has reached the very exciting stage of having the potential of being quantitatively descriptive of simple phenomena and qualitatively descriptive of complex phenomena. Attaining the goal of complete quantitative predictability, however, is hampered by the lack of comprehensively developed and validated chemical kinetic and transport data base relevant for high-temperature chemically reacting flows involving the oxidation of complex fuels. The proposed microgravity experiments on the aerodynamically clean, burner-generated spherical diffusion flames are expected to yield high-quality diffusion flame data that, together with those acquired from homogeneous and premixed flame experiments, will provide the needed information and constraints for such a development and validation. It is to be emphasized that the one-dimensional spherical diffusion flame is probably the most desirable flame configuration for a study of this nature, and that this flame is only realizable in the microgravity environment.

In the course of developing and validating the fundamental data sets, our proposed experiments and the associated computational simulations will be concurrently yielding quantitative and qualitative understanding on various elemental flame phenomena. For example, by studying the motion of diffusion flames, we will be able to further scrutinize the universal importance of fuel accumulation, which was originally found to be important in droplet burning. Furthermore, by requiring quantitative predictability of the flame motion, we will be able to assess the importance of radiation loss and re-absorption. Other phenomena to be studied include the potential onset of pulsating and cellular instabilities in near-limit situations and their influences on flame extinction, and soot formation. It is noted that each of these phenomena is a major area of study in its own right, and the quality and meaningfulness of the study can be greatly facilitated in microgravity environments.

It is important to emphasize that while a major goal of the present investigation is to acquire accurate data on phenomena affected by chemistry such as extinction, experiments performed in ground-based low-gravity facilities could not unambiguously demonstrate the occurrence of

extinction. Furthermore, while extinction was indeed observed in the 1-g, low-buoyancy experiments, the many special provisions (low-pressure, low molecular-weight fuel, inverse flame) required to achieve micro-buoyancy render the experimental results of limited utility in terms of kinetics studies. Long-duration, space-based experiments are therefore needed.

The last point we wish to mention is the proper strategy needed to tackle a research project of the present nature, one that has an excessively long lead time before the first experimentation can be conducted. It is important that during the time leading to the space experimentation, auxiliary ground-based experiments complemented by computational and analytical developments are simultaneously conducted so as to produce as much supplemental information as possible in anticipation of the eventual harvesting of the space-based data. Our low-buoyancy burner was developed precisely with this objective in mind, and its usefulness has been repeatedly demonstrated. Furthermore, while a substantial component of our program is based on qualitative and quantitative verification, it must be recognized that some of the mechanisms and transport parameters to be "validated" could actually be evolving with time. Consequently the validation must be conducted against the most current information that is available at the time the space data are acquired. An example is the soot formation kinetics. It would be ignorant of us to attempt to validate our space data against any mechanism that is available at the time this document is prepared. It is precisely for this reason that we have purposefully not mentioned any specific kinetic mechanisms for validation because with the rapid rate with which research in this area is progressing, it is certain that our understanding will be very different in several years. In order to be maximally benefited by costly endeavors associated with space experimentation, one has to be informed and current in terms of knowledge, and agile in adaptation and execution.

1.5 Journal Publications Resulting from Current Investigation

1. "Role of flamefront motion and criterion for global quasi-steadiness in droplet burning," by L. He, S.D. Tse, and C.K. Law, *Proc. Comb. Inst*. **27**: 1943-1950 (1998).
2. "On micro-buoyancy spherical diffusion flames and a double luminous zone structure of the hydrogen/methane flame," by C.J. Sung, D.L. Zhu, and C.K. Law, *Proc. Comb. Inst.* 27: 2559-2567 (1998).
3. "A computational study of the transition from localized ignition to flame ball in lean hydrogen-air mixtures," by S.D. Tse, L. He, and C.K. Law, *Proc. Comb. Inst.* 28: 1917-1924 (2000).
4. "Microgravity burner-generated spherical diffusion flames: experiment and computation," by S.D. Tse, D.L. Zhu, L. He, C.J. Sung, and C.K. Law, *Combust. Flame* 125:1265-1278 (2001).
5. "Oscillatory extinction of spherical diffusion flames: micro-buoyancy experiment and computation," by S.W. Yoo, E.W. Christiansen, and C.K. Law, *Proc. Comb. Inst.* 29: 29-36 (2002).
6. "Chemiluminescent OH and CH flame structure and aerodynamic scaling of weakly buoyant nearly spherical flames," by S.W. Yoo, C.K. Law, and S.D. Tse, *Proc. Comb. Inst.* 29: 1663-1670 (2002).
7. "Dynamics of flame ball formation from localized ignition: effects of elevated pressure and temperature," by J. Yuan, S.D. Tse, and C.K. Law, *Proc. Comb. Inst.* 29: 2501-2508, (2002).
8. "A computational study of oscillatory extinction of spherical diffusion flames," by E.W. Christiansen, S.D. Tse, and C.K. Law, *Combust. Flame* 134: 327-337 (2003).

9. “Response of spherical diffusion flames under rotation with general Lewis number,” by S. Yoo, J. Qian, J. K. Bechtold, and C. K. Law, *Combustion Theory and Modeling* 9: 199-217 (2005).
10. “Porous spherical burner for combustion experimentation,” by S.W. Yoo, D.L. Zhu, and C.K. Law, *Review of Scientific Instruments* 77, No. 7, Art. No. 075102 (2006).
11. “Effects of variable density on response of spherical diffusion flames under rotation,” by S.W. Yoo and C.K. Law, *International Journal of Heat and Mass Transfer* 50: 2924-2935 (2007).
12. “A mechanistic study of Soret diffusion in hydrogen–air flames,” F. Yang, C.K. Law, C.J. Sung, and H.Q. Zhang, *Combust. Flame* 157: 192–200 (2010).

2.0 FLIGHT EXPERIMENT

2.1 Objectives of the Flight Investigation

Current experimental and theoretical capabilities make detailed, quantitative descriptions of laminar flames situated in well-defined flow fields conceivable provided that comprehensive chemical-kinetic and transport mechanisms are available. The comprehensiveness of these mechanisms has been extensively tested for premixed but not diffusion flames, especially in simple, well-defined flow fields not complicated by buoyant flows. A burner-generated spherical diffusion flame provides a simple, one-dimensional flame geometry that permits a rigorous comparison between detailed theory and experimental verification. Existing theory and limited low-gravity experimental results suggest that quasi-steady spherical diffusion flames can exist with some combinations of fuel mixture supply rates and quiescent ambient oxidizers. With respect to the steady flame conditions, altering fuel supply rates to limit flame residence time induces a convective-kinetic extinction limit. Alternatively, very large residence times allow radiative heat losses and diffusive transport mechanisms to quench the flame. Near these dual flammability boundaries of quasi-steady flames, flame-front instabilities may appear before the flame is quenched.

We seek to investigate and improve the fidelity and comprehensiveness of the chemical kinetic mechanisms and transport submodels used in the simulation of aerothermochemical phenomena, and consequently identify possible modifications, by characterizing important unit combustion processes, including: (1) the dynamics and extinction of diffusion flames, with emphases on fuel vapor accumulation, radiation heat transfer, flame pulsation, and flame kinetics; and (2) the structure and response of characteristically sooty flames, with emphases on flame front stability and soot formation. Comprehensive predictive capability can be achieved by employing the simple flames of Process (1) to interrogate and suggest modifications of the kinetic and transport data bases, and then validate their adequacy in the chemically and aerodynamically more complex situation of Process (2).

A series of experiments is proposed with the following specific objectives, in both soot-free and sooty flames, to compare with detailed computational simulation to assess transport properties and detailed chemical kinetics (including chemiluminescence):

Objective A. Measure and characterize the transient structure (such as temperature and species distribution) of diffusion flames established at initially non-steady, spherical flame structures for mixtures of different H_2/CH_4/diluent ratios (soot-free) and different C_2H_4/diluent ratios (sooty), for different flow rates.

Objective B. Determine the quasi-steady convective/chemical-kinetic extinction limits (low system Damkohler numbers) and radiative/chemical-kinetic extinction limits (high system Damkohler numbers) for mixtures of different H_2/CH_4/diluent ratios (soot-free) and different C_2H_4/diluent ratios (sooty).

Objective C. Determine the existence (for different Zeldovich number, Ze), onset (as a function Da), and nature (i.e. mode, frequency, amplitude) of pulsating instabilities theoretically predicted to occur in transient spherical diffusion flames using fuel/diluent mixtures that are above a critical Lewis number.

2.2 Approach

A series of experiments is proposed in which mixtures of various gaseous fuels and diluents will be issued into an oxidizing environment through a spherical porous burner and ignited to obtain, nominally, a spherical, one-dimensional stabilized flame. Synchronized measurements are to be made including spectrally resolved images, flame and burner temperatures, radiative flux measurements, and system operating conditions (including reactant flow rates, ambient temperatures, pressures and acceleration levels, etc.). These data are to be used for comparisons of flame behavior and structure with detailed numerical simulations of the flames.

Conventional gaseous fuels including hydrogen, methane, and ethylene will be used. Hydrogen is the simplest fuel and its reaction mechanism is also reasonably established. Methane is the simplest hydrocarbon and extensive studies have been conducted on its combustion chemistry. Ethylene is a typical sooty fuel and is also an important intermediate for the oxidation of higher hydrocarbons. Diluents mixed with fuel are to include nitrogen and helium to adjust mixture diffusivities, and carbon dioxide to influence flame radiation characteristics.

2.2.1 Flame Front Motion

To address the first experimental objective, fuel/diluent mixtures will be issued from the spherical burner and ignited at flow rates expected to form flame fronts that move toward idealized steady-state conditions. As the flame front moves, transient measurements of the flame front velocity and flame structure will be obtained using the imaging and radiometric systems. The flame characteristics will be compared with predictions of the transient numerical simulation of spherical diffusion flames for evaluations of detailed chemical kinetic and transport sub-models.

2.2.2 Dual Quasi-Steady Extinction Limits at Low and High System Damkohler Numbers

The second experimental objective will be addressed in two parts, one each for low and high system Damkohler number (Da) extinction-limit determinations. To observe convective/chemical-kinetic extinction at low Da, fuel/inert mixtures will be issued from the spherical burner and ignited at initial flow rates expected (or known/observed) to form flames that evolve toward idealized steady-state conditions. Following ignition and initial flame front movement, the fuel/inert flow rate will be abruptly reduced to a second flow rate below the expected extinction limit. The quasi-steady extinction is expected to occur as the flame adjusts to the reduced flow rate. To refine the determination of the extinction flow rate for each fuel/diluent mixture, repeated tests are to be conducted at successively lower initial flow rates and higher secondary flow rates.

To observe radiative/chemical-kinetic extinction at high Da, fuel/inert mixtures will be issued from the spherical burner and ignited at flow rates *above and beyond* those expected (or known/observed) to form steady flames when radiative loss is considered. The quasi-steady extinction is expected to occur as the flame front moves outward before reaching the theoretical, practically-non-attainable *adiabatic* steady-state radius.

At the low Da extinction limit, chemical kinetic rates will be retarded with respect to flow rates by diluting the fuel stream with an inert gas that acts to decrease the flame temperature. Inert dilution acts in principal to increase the extinction flow rate. Based on theoretical predictions, fuel/inert mixtures are to be chosen for which the extinction flame radius is large enough to minimize the effects of heat loss to the burner. The surface temperature of the burner will be directly measured to quantify this loss.

At the high Da extinction limit, rates of radiative emissions from the flame and radiative reabsorption elsewhere are to be accentuated in some cases by using a radiatively active diluent such as CO_2, recognizing the fact that it is chemically active as well. Sooty fuels could also be used to

enhance radiative losses, but the participation of CO_2 can be more readily incorporated into the detailed chemical kinetics and radiative transport of the numerical simulation than soot mechanisms.

Transient measurements of flame behavior and structure will be obtained as the flame approaches extinction using the imaging and radiometric systems. The flame characteristics will be compared with the predictions of the transient numerical simulation of spherical diffusion flames for evaluations of detailed chemical kinetic and transport models.

2.2.3 Flame Front Instabilities in Non-Premixed Flames

The third experimental objective will be addressed in two parts since pulsating flame front instabilities are predicted to occur near the extinction conditions at both low and high Da. The approach taken to facilitate observations of the instabilities is similar to the approach for observing extinction except fuel/diluent mixtures with large system Lewis numbers (Le) are used.

To observe pulsating flame front instabilities near the low Da limit, fuel/inert mixtures with large Le (e.g. dilution with He) will be issued from the spherical burner and ignited at initial flow rates expected (or known/observed) to form flames that evolve and reach steady-state conditions. Following ignition and initial flame front movement, the fuel/inert flow rate will be abruptly reduced to a second flow rate below the expected extinction limit. Instabilities are expected to develop as the flame adjusts to the reduced flow rate. To refine the determination of the unstable condition for each fuel/diluent mixture, repeated tests are to be conducted at successively lower initial flow rates and higher secondary flow rates.

To observe pulsating flame front instabilities near the high Da limit, fuel/inert mixtures with large Le (e.g. dilution with He) will be issued from the spherical burner and ignited at flow rates *above and beyond* those expected to form flames that evolve and reach steady-state conditions with radiation. The instabilities are expected to develop as the flame evolves past an unstable condition and then quenches due to radiative loss. To refine the determination of the unstable condition, repeated tests are to be conducted at successively lower flow rates.

Additionally, radiative losses have been shown to promote instabilities. To assess the influence of radiative loss, fuel/diluent mixtures with diluents of different radiative properties (e.g. CO_2) will be used.

Transient measurements of flame behavior and structure will be obtained using imaging and radiometric systems as the flame approaches unstable conditions. Since theoretical pulsating oscillations can occur at frequencies higher than conventional imaging frame rates (Yoo, 2002), high frequency sampling of radiometer signals will be used to detect them. Flame characteristics and the specific conditions leading to flame front instability will be compared with the predictions of the transient numerical simulation of spherical diffusion flames for evaluations of detailed chemical kinetic and transport models.

2.2.4 Dynamics of Characteristically Sooty Flames

To address the experimental objectives with respect to the response of diffusion flames that are characteristically sooty to an initially non-steady-state condition, ethylene will be issued from the spherical burner and ignited at flow rates expected to form flames that evolve under quasi-steady conditions. The fuel and inert concentrations for the C_2H_4/inert are varied to address different fuel concentration effects on sooting, along with corresponding radiation. Since the characteristic residence time will affect sooting tendencies, two flow rates are investigated that correspond to two flame locations. The onset of soot formation will be determined by the imaging and radiometric systems. The influence of thermophoretic transport of the soot particles will be assessed from the

relative motions of the flame front and the soot layer. The role of soot in flamefront motion, radiative heat loss, and flamefront instability will be specifically examined.

2.3 Science Data End Products

The Science Data End Products (SDEPs) are the graphs, analyses, and correlations, which meet the science objectives, for which we anticipate to publish after the flight experiment. All of the experimental data will be analyzed in comparisons with simulations. The SDEPS are listed below, in Table 2.3, which presents the objectives, the associated SDEPs, and the raw data needed. Much of the data collected, as well as SDEPs, are intertwined in meeting various objectives. As such, the raw data sets corresponding to the science objectives are presented in Table 3.6 to give a better picture of how specific experiments in the test matrix meet the objectives.

Table 2.3 Science Data End Products

Experiment Objective	Science Data End Product (SDEP)	Raw Data Needed
A) **Flame Structure Evolution**: Measure and characterize the transient structure of diffusion flames established at initially non-steady, spherical flame structures for mixtures of different H_2/CH_4/diluent ratios (soot-free) and different C_2H_4/diluent ratios (sooty), for different flow rates.	1) **Sequence of color and OH* images of the flame as a function of time, flow rate, and fuel composition**. Sequence of photos of visible flame emission will be shown to exemplify the dynamics of the flames in the experiment.	1a) Color images 1b) UV images
	2) **Visible flame radius as a function of time, flow rate, and fuel composition**. Transient data of flame radii (based on chemiluminescence or soot emission) as a function of time for different mixtures and inerts will be compared to numerical simulations to assess the validity of chemical kinetics (including those for electronically-activated species) and transport. The quasi-steady nature of the flame spread process will be assessed.	2a) Color images 2b) UV images
	3) **Temperature (and desired major species) radial distribution as a function of time, flow rate, and fuel composition**. All phenomena examined should be analyzed based on this data, along with computational simulation. Evolution of the flame structure will impact the spreading behavior, and thus flamefront motion (SDEP 1). The flame structure at extinction will reveal the mechanisms involved (e.g. radiative vs kinetic).	3a) Temperature profiles
	4) **Soot onset (determined from visible luminescence versus soot extinction measurements) as a function of radii for different flow rates and fuel compositions**. Soot onset dependence on local temperature and fuel concentration will be examined for quasi-steady	4a) Color images 4b) Soot volume fraction measurements 4c) Temperature

	conditions.	profiles
B) **Dual Extinction Limits at Low and High System Da**: Determine the quasi-steady convective/chemical-kinetic extinction limits and radiative/chemical-kinetic extinction limits for mixtures of different H_2/CH_4/diluent ratios (soot-free) and different C_2H_4/diluent ratios (sooty)	1) **Extinction limits as a function of system Damkohler number**. Turning points in the plot of maximum temperature as a function of mass flow rate will identify the quasi-steady extinction limits.	1a) Temperature profiles 1b) Color images 1c) UV images 1d) Mass flow rate
	2) **Total radiative loss as a function of radius for different flow rates and fuel compositions.** Compared with heat release rate derived through simulations, the ratio will help to assess quasi-steady extinction characteristics.	2a) Radiometer data 2b) Color Images, 2c) UV Images 2d) Temperature profiles
	3) **Peak CH* or OH* chemiluminescence along with peak temperature as a function of radius, for different times, flow rates, and fuel compositions**. This data will assess the correspondence of chemiluminescence with heat release, of transient versus quasi-steady extinction, and of maximum temperature versus maximum chemiluminescence. Data will be compared with numerical simulations to assess the validity of chemical kinetics for chemiluminescence reactions.	3a) UV images (filter corresponding to CH* is desired) 3b) Temperature profiles
	4) **Radiation loss versus time for sooty flames, for different flow rates and fuel compositions.** This SDEP will assess radiative loss from soot emission. Thermophoretic and convective transport of soot will be assessed.	4a) Radiometer data 4b) Color images 4c) Temperature profiles
C) **Flame Front Instabilities in Non-Premixed Flames**: Determine the existence, onset, and nature of pulsating instabilities theoretically predicted to occur in transient spherical diffusion flames using fuel/diluent mixtures that are above a critical Le.	1) **Total chemiluminescence as a function of time**. This SDEP will identify instability near extinction where the flamefront may move negligibly.	1a) PMT data
	2) **Total radiative loss (based on radiation flux) as a function of radius, for different flow rates and fuel compositions**. This SDEP will identify instability near extinction where the flamefront may move negligibly.	2a) Radiometer data 2b) Color Images, 2c) UV Images 2d) Temperature profiles
	3) **Oscillation mode, frequency, and amplitude near extinction as a function of flow rate for flames of different Le and mass flow rates** will be mapped.	3a) Radiometer data 3b) PMT data 3c) Mass flow rate
	4) **Comparison of extinction times and extinction radii as a function of flow rate, for different fuel compositions**. (based on radiometer data,	4a) Radiometer data 4b) PMT data

	temperature, and UV emission). Different criteria for extinction will be examined. Radiometer data is expected to capture non-quasi-steady extinction. Local temperature will assess actual extinction, while UV emission will assess chemiluminescence prior to extinction. Transient versus quasi-steady flames will be assessed.	4c) Color images 4d) UV images 4e) Temperature profiles
	5) **Soot radial distribution as a function of time for different flow rates and fuel compositions during fully transient flame front movement**. Soot dynamics and dependence on local temperature and fuel concentration will be examined for fully transient or unsteady conditions.	5a) Color images 5b) Temperature profiles 5c) Soot volume fraction measurements

2.4 Anticipated Knowledge and Value to be Gained

These experiments are expected to contribute rigorous benchmark data with which to evaluate the adequacy of existing chemical kinetics and transport models, especially including radiative transport, in predicting the behavior of diffusion flames. More specifically, the following phenomena and flame characteristics are sought:

1. The transient and steady state behavior and structure of spherical diffusion flames.
2. Quantitative determination of the states of flame extinction, especially the dual extinction modes at high and low system Damkohler numbers.
3. Identification and quantitative characterization of the theoretically predicted flame front oscillations prior to diffusion flame extinction.
4. The transient and steady state behavior and structure of sooting spherical flames.
5. Residence time effect on soot formation, with only curvature effects and no strain.
6. The effects of soot radiation and transport on extinction, at constant mass flow rate.

2.5 Justification for Extended Duration Microgravity Environment

2.5.1 Limitations of Terrestrial (1g laboratory) Testing

We seek to make observations of truly one-dimensional flames whose structure can be studied without complications due to uncertainties in the flow pattern caused by buoyancy. Such fundamental study of flame structure and dynamics is best served via the elimination of buoyancy through the reduction of gravity.

The minimum sizes of these flames imply that buoyancy would be significant if the experiments were conducted in normal gravity. Previous experimentation on earth has amply demonstrated this influence. Although studies of spherical diffusion flames were conducted in normal gravity using the low-pressure, inverse-flame arrangement (see §1), the conditions are limited for small flames, low pressures, low molecular weight fuels. Indeed, only the hydrogen flame can be considered to be

nearly buoyancy free. With such constraints, normal-pressure, micro-gravity, hydrocarbon-based experiments are requisite.

One-dimensional spherical flames allow for the unambiguous study of such fundamental flame phenomena as the dynamics and extinction of diffusion flames (including the mechanisms of flame front unsteadiness), soot suppression/formation, and flame front instabilities, without gravity-induced baroclinicity and buoyancy, on the flame responses.

2.5.2 Limitations of Drop Towers and Aircraft

Extensive experimentation has been conducted in the 2.2-s drop tower, 5-s drop tower, and parabolic aircraft, as reviewed previously in §1.3. Although experimental data of good quality were obtained on the transient response of spherical diffusion flames in the 2.2-s drop tower facility, the duration was insufficient to observe radiative extinction. The numerical simulations indicate that, for the characteristic flames under study, more than 2.5s of microgravity time is needed. Subsequent parabolic aircraft experimentation afforded the additional low-gravity duration (up to 10s by free-floating the apparatus), as well as an experimental package incorporating rainbow schlieren (which cannot be contained within a package for the 2.2-s drop tower), although radiative extinction was still not observed. The unavoidable g-jitter associated with the facility, however, renders the observation less definitive. Note that even though the package was free-floated, umbilical restrictions could not be avoided. This g-jitter effect was substantiated by accelerometer data. 5-s drop tower experiments for a mixture composition of 20%H_2 / 25%CH_4 / 55%N_2 did show events with local extinction toward the end of the drop (see Fig. 1.11). While these new results are extremely encouraging and suggest that radiative extinction can indeed be experimentally observed, the 5-s duration is still insufficient. To obtain spherical symmetry for small burners (in order to minimize heat loss to the burner), as well as to ensure quasi-steady flame evolution up to radiative extinction (for the flame sizes to be studied), low mass flow rates are needed, which increase the characteristic time needed. Moreover, for other mixture compositions (such as 50%H_2/10%CH_4/40%N_2 45%H_2/55%N_2), more than 5s of microgravity duration has been computationally predicted to be needed to achieve radiative extinction (see Fig. 1.12). Additional time is also needed to employ multi-staged flames (where the mass flow rate is changed) so that such phenomena as kinetic extinction can be studied (for example, by establishing a quasi-steady flame at a given flow rate and then reducing it so that the flame front moves inwardly and quasi-steadily until kinetic extinction). Finally, given the characteristic time for diffusion flame oscillation (see Fig. 1.14), which does not occur until the flame nears the quasi-steady extinction limits, extended microgravity duration becomes essential in order to study the phenomenon.

2.5.3 Justification for Space-Flight Facility

As explained above, extended microgravity duration, of high quality, is needed to make all necessary flame structure measurements, allowing for the study of transient phenomena (such as flame oscillations and fuel vapor accumulation) and extinction processes. Moreover, at present, the advanced diagnostics found on the space-flight facility cannot be utilized in the drop tower facilities. Numerical simulations indicate that about 25s of microgravity is needed for non-extinguishing flames to reach 80% of their steady-state radius, for the fuel mixtures and flow rates examined. It is expected that within this duration, the aforementioned phenomenon can be duly investigated. The total experimental duration for a single case would be 25s. This duration is within the 25s bound imposed by constant volume combustion within the specified CIR dimensions (see §Appendix 5.1) regarding oxygen depletion for a "penetration depth" of 20cm.

2.6 Mathematical Modeling and Analysis

Recall that the essential motivation for the proposed program is to exploit the buoyancy-free environment of microgravity so that the resulting spherically symmetric, one-dimensional flow is the simplest possible. Consequently there is no ambiguity and complexity in the description of the flow field. Together with the system being purely gaseous, these features allow the tight and meaningful coupling between experiment and computation for the present study. That is, if the chemistry, diffusive transport, and radiative transport descriptions of the system are accurate, and if the experimental data are accurate, then they should compare well with each other. There are two implications from the above expectation. First, we can study the various issues related to the flame structure and dynamics mentioned earlier with confidence and unusual clarity, from both theoretical and experimental results. Particularly, it is recognized that the experimental results will be limited considering the time available for experimentation onboard the ISS. However, once we can establish that our model can indeed simulate the experiment, further exploration of the phenomena of interest can be conducted computationally. Second, if there are some deficiencies in the chemistry and transport sub-models, it is sometimes possible to use the experimental data to identify the source of such deficiencies and offer potential remedies. One example of such an approach, not related to microgravity studies, is the use of the experimentally determined laminar flame speed to optimize the kinetic mechanisms of hydrocarbon fuels.

The transient numerical simulation of spherical flames developed as part of this program includes detailed chemistry and transport models, especially radiation mechanisms. Each description of the flames obtained from the experiment, including measurements of aspects of the flame structure, growth or flame front velocities, and the specific test conditions where steady state flames, flame extinctions, flame front instabilities, soot suppression limits, etc., comprise a rigorous test of the detailed model. Together they provide a measure of the comprehensiveness of the chemical kinetic and transport models.

The numerical simulation is also being used as a predictive tool to develop the science requirements for this experiment, especially the collection of test conditions and most aspects of the measurement systems. Due to time and g-jitter limitations, little of the planned test matrix can be adequately explored in the ground based test facilities, and the flight experiment definition will rely on the best effort in the modeling work.

Post flight comparisons of the experimental results with the preflight numerical simulations will lead to an assessment of the component models of the simulation. Discrepancies will be explored within the limits of the accuracy range of the model constants obtained from the literature. If the comparisons are unsatisfactory, additional sensitivity analyses using the simulation may be indicated to identify the important reactions and separate kinetics studies may be needed.

3.0 EXPERIMENT REQUIREMENTS

3.1 Requirements Discussion

This section does not include any requirements, but instead describes their importance in achieving the experiment objectives. The requirements have been incorporated into the merged *ACME Science Requirements*.

3.1.1 Experiment Configuration Requirements

3.1.1.1 Spherical Burner

The burner will produce flames (up to 4cm radius) with spherical and concentricity characteristics meeting or exceeding that presently capable of the spherical burner presently provided by the PI. The burner design includes the spherical, porous burner and the supply tube.

3.1.1.2 Gas Supply

Studies will be conducted with gaseous fuels, i.e., hydrogen, methane, and ethylene, all diluted with inert(s). Additional inert(s) can be variably introduced into the final fuel mixture stream.

The fuel/inert mixtures in the experiment include both H_2 and CH_4, or H_2 or CH_4 alone, aimed at addressing chemical kinetic aspects. The inert concentrations are all fixed at 55% for all tests for baseline comparison. Higher flow rates are used to examine radiative extinction. Ramping down to lower flow rates are used to examine kinetic extinction. Flame sooting experiments utilize C_2H_4. The fuel component (C_2H_4) concentration is varied from 20-30%. Since characteristic residence time will affect sooting tendencies, two flow rates are investigated.

The use of the different inerts, i.e. N_2, He, CO_2, will alter the characteristic flame temperature and radiative properties, affecting extinction characteristics. Additionally, since the different inerts directly affect the diffusive properties (and radiative heat loss), flame stability issues can be addressed.

The oxidizing atmospheres will be 21% O_2 based, simulating "normal air." The balancing inerts will correspond to the same used for the fuels.

3.1.1.3 Burner Gas Delivery

Flow system shall deliver fuel, inert(s), and oxygen to the burner, in the various combinations as stipulated in the Test Matrix (see §3.3). System must allow different total-flow rates and mixture compositions to be delivered to the burner during the course of a single test. One test is estimated to last less than 25s. A requirement to provide gas at the maximum flow rate for at least 25s has been established.

Flow control of fuel during testing is required. In some tests, flow rates change within the course of the test.

For a consistent basis of comparison, as well as well-defined modeling conditions, the supply temperature of fuel mixture shall be the same for all tests. Fuel supply temperature affects the flame temperature and hence extinction characteristics.

3.1.1.4 Ignition

The ignition system (*e.g.* a hot wire) shall ignite the fuel dispensed from the burner within the specified flow ranges, at approximately 3 mm from the burner surface. 50W for 200 ms have been shown in drop-tower studies using hot wire to properly ignite the mixtures to be investigated. Since the fuel/oxidizer concentration at the igniter is not known a priori for such diffusion flames, ground-based testing is to be conducted to verify the ignition parameters. An ignition system with sufficient power shall be required. Depending on the actual ignition system to be utilized, a maximum power requirement will be determined to ensure minimal effects on subsequent flame behavior, as well as practical considerations such as wire burnout. Having the flame initially situated near the burner surface, the flame structure is of limited size, providing a clear initial condition for computational and theoretical modeling.

A retractable igniter shall accomplish ignition. Flame disturbance during deployment and retraction of ignition system (e.g., induced wakes, heat transfer into mechanism) should be minimal. Igniter should retract out of performance volume.

3.1.1.5 Ambient Environment

The chamber air shall be dry with an initial oxygen mole fraction corresponding to that for medical dry air. In order to accurately quantify the combustion species it is important that the initial composition of the chamber atmosphere is precisely known. This requirement ensures that the results of the experiment are not affected by contaminants such as particulate, moisture, or trace presence of other species. Furthermore, it is important to ensure that each test point is performed with the same starting conditions in order to allow each test point to be "cross referenced" to other test points and to allow for accurate model correlation. Of particular importance is the starting O_2 concentration in the chamber prior to each test.

In the interest of conserving valuable gas resources, the initial ambient gas composition may be established by scrubbing the chamber atmosphere between tests as long as repeatable initial conditions are achieved. In this case, ambient concentrations of CO_2, H_2O, other combustion products, and unburned fuel must be reduced to below 0.02% mole fraction combined. For the "CO_2-air" cases, H_2O, other combustion products, and unburned fuel must be reduced to below 0.02% mole fraction combined.

For a consistent basis of comparison, as well as well-defined modeling conditions, the initial ambient pressure shall be the same for all tests. Chamber pressure can vary from 101325 Pa to 303975 Pa (i.e. 1 to 3 atm) during constant volume combustion. It is desirable to limit pressure increase because pressure affects the thermal diffusivity, density, radiative properties, and chemical reaction rates.

For a consistent basis of comparison, as well as well-defined modeling conditions, the initial ambient temperature shall be the same for all tests. Ambient temperature affects the flame temperature and hence extinction characteristics.

The specified free volume allows up to 25s of constant volume flame evolution without a drop in oxygen concentration at 20cm radius (see §Appendix 5.1). Such duration has been deemed sufficient to study the aforementioned flame responses.

Chamber volume should be sufficient to allow a spherical flame field to develop in a manner that is not affected by the chamber walls. The specified dimensions of volume should allow for

sufficient distance from the chamber walls to the flame zone so that species and temperature gradient fields are not affected (see §Appendix 5.1).

The large volume of hot gas present in the flame front is very sensitive to disturbance by accelerations, characterized by large Grashof numbers. The maximum allowable acceleration is set by the need for the expected local buoyancy-induced flow velocity to be smaller than the local fuel flow rate velocity. See §Appendix 5.5.

Currently, there are requirements for emission measurements, e.g. with PMTs in the UV and visible. However, knowing the actual emissivity values for the chamber walls and all other internal surfaces in direct view of the flame is important because it can affect radiative transport to/from the flame. The requirements for UV and visible wavelengths is based on avoiding reflections that would impact imaging quality. The requirement at IR wavelengths is to mimic a large system by avoiding multiple passes of radiation corresponding to photon emission from the combustion product species through the flame zone. Having a high emissivity greatly simplifies radiation modeling. It is desired that actual spectral emissivity values of the internal surfaces are provided to the PI.

3.1.2 Monitoring Measurements Requirements

3.1.2.1 Chamber Pressure

The measurement of ambient pressure in the chamber is needed to understand the quasi-steady conditions of the test and the knowledge of the chamber gas pressure. Measurements of the ambient pressure during constant volume combustion are requisite to assess its impact on thermal diffusivity, density, radiative properties, and chemical reaction rates.

3.1.2.2 Chamber Oxygen Concentration (Desired)

The O_2 concentration near the chamber "wall" and at a 10cm radius is desired to be measured. These boundary conditions are important for modeling purposes. 10cm radius corresponds to the "free area" performance volume specification. Measurements of the oxygen concentration near the chamber wall assess the size of the flame structure, as well as oxygen depletion effects on the flame.

3.1.2.3 Gas Flowrates

Measurement of the gas flow rate issuing from the burner is a requisite boundary condition for the problem.

3.1.2.4 Acceleration

Flame Front Motion—Measurement of acceleration is needed in order to determine if changes in the flame front velocity or flame shape are due to acceleration or some other factor. Continuous measurement of the g-vector will correlate any buoyancy induced flame response, e.g. g-jitter.

Quasi-Steady Extinction—Continuous measurements of the g-vector will correlate any buoyancy induced altering of the flame dynamics and structure, affecting the extinction limits.

Instability and Extinction—Continuous measurement of the g-vector will correlate any buoyancy-induced instability.

Sooty Flames—Continuous measurement of the g-vector will correlate any buoyancy induced flame response directly affecting soot formation and transport.

3.1.3 Science Diagnostics Requirements

3.1.3.1 Optical access

A minimum of two views along orthogonal axes (normal to support axis of burner) of the spherical flame is required in order to allow flame imaging and optical diagnostics, and to assess symmetry. Imaging and optical diagnostics systems include color imaging and UV imaging. All windows shall allow for light transmittance in the specified wavelength range of the corresponding imaging equipment.

3.1.3.2 Color Imaging

Spatial distribution history of visible emission (0.4 μm to 0.7 μm) from the flame shall be imaged from one and if possible, two (2) orthogonal views. The required field of view (FOV) is 120 mm in diameter, and an adjustable iris or gain is needed to accommodate varying flame intensities. In addition to flame radius and shape from visible chemiluminescence, some soot formation and extinction processes should be observable from visible incandescence. The perpendicular views characterize the symmetry of the flame. The field of view is set by the need to resolve the largest flames anticipated, and the framing rate is set by the need to resolve the fastest events anticipated.

Flame Front Motion—Measurement of the visible radiation from the flame assesses flame symmetry and visible "flame radius" to be compared with peak temperature and peak heat release rate locations. Possible soot formation and extinction processes can be assessed from incandescence. Since the visible images will not be deconvoluted (as with case of the UV images), the focal depth of the system shall be kept as narrow as possible to ensure imaging of the flame at its cross-sectional center "plane."

Quasi-Steady Extinction—Lack of visible flame radiation is not a good indicator of flame extinction. See Tse *et al*. (2001). The possible discrepancy between the intensity of visible flame radiation and magnitude of temperature of the field of the flame structure will be compared.

Instability and Extinction—Visible "flame radius" oscillation may be captured. Image allows for assessment of flame instability induced by the edge flame created by the burner support tube.

Sooty Flames—In addition to "flame radius" and shape from visible chemiluminescence, soot presence should be observable from visible incandescence.

3.1.3.3 UV Imaging

Ultraviolet imaging of gas-phase chemiluminescence provides information on the spatial and temporal distribution of intermediate product species, i.e. OH* at 310 nm (presently planned) or CH* at 431 nm (highly desired)). Ultraviolet imaging will capture hydrogen/oxygen/inert flame

images, which cannot be visualized using direct color imaging. This requirement will be met by using the CIR's Low Light Level UV (LLL-UV) Camera Package. The LLL-UV package covers the spectral range of 200 – 750 nm but will launch with a filter for viewing only the OH* line at 310 nm.

Species concentrations within the flame structure are needed to compare with the detailed chemistry computations. Moreover, OH* emission from the flame often corresponds to the peak heat release position, thereby providing the flame location.

Flame Front Motion—UV imaging of chemilluminescence from electronically excited species such as OH* (for all fuels mixtures) and CH* (for fuel mixtures containing elemental carbon) provides for the assessment of both detailed chemistry and (to a much lesser degree) flame structure, when compared with the computational simulations. Axisymmetric Abel deconvolution of the projection image of the flame chemilluminescence within the focal depth of the camera (with appropriate narrow band filters) produces a map of excited species concentration as a function of radius (see §Appendix 5.4). Comparisons with computational simulations will allow for possible refinement of the kinetic parameters associated with the formation of these excited species, as well as the extrapolation of the distribution of the non-excited species (for further flame structure assessment). The peak locations of these excited species will be tracked and compared with peak heat release rate location (from computations) and peak temperature (from experimental measurement and computations).

Quasi-Steady Extinction—Measurements of OH* or CH* field, when compared with computational simulations, provide for the assessment of the chemistry near the extinction state.

Instability and Extinction—Measurements of OH* or CH* field allow tracking of the flame front near the peak heat release location.

Sooty Flames—Measurements of the OH* or CH* fields are needed to assess the reaction zone profile of the flame structure. Such measurement allows for the identification of the onset of sooting as the flame expands outward from a non-sooty one to a sooty one.

3.1.3.4 Spherical Burner Temperature

Transient measurement of the burner surface temperature provides a requisite initial and boundary condition for the problem. The temperature at the burner surface assesses the heat transfer to the burner, which affects the flame temperature and hence extinction characteristics. Moreover, in order to perform an accurate energy balance it will be necessary to quantify heat transfer from the flame, requiring accurate measurements of the temperature at the burner surface.

3.1.3.5 Gas-Phase Temperature Distribution

The diagnostic should allow for determination of peak temperature position, as well as provide flame structure information. The final diagnostic should provide the density/temperature field (1-D radial is sufficient) history, so that *local* assessment of extinction can be made (based on the precipitous drop in temperature).

Flame Front Motion—Measurements of the temperature/density field are requisite to assess the transient flame structure. Analyses (Tse et al. 2001) have shown that transient response of the flame is dependent on the flame structure rather than simply the flame front radius. Flames

with the same flame front radius can possess vastly different flame structures; for example, compare the infinitely large diffusion flame structure at steady state with the localized one at ignition. The experimental data will then be directly compared to the transient computational simulations for both density and temperature distribution. Additionally, from a mapping of the temperature/density profile, the location of peak temperature can be easily identified and tracked. Analyses have shown that for above atmospheric pressure, the location of peak temperature, rather than that of peak chemiluminescent emission (Tse et al. 2001), corresponds well with the location of peak heat release rate, for the mixtures examined. As a result, the location of peak temperature shall be taken to be the flame front radius, one of whose transient response will be examined.

Quasi-Steady Extinction—Measurements of the temperature field are critical for the assessment of the moment of flame extinction. Analyses (Tse et al. 2001) have shown the lack of correspondence between chemiluminescent flame intensity and actual flame strength (as described by flame temperature and heat release rate). For example, chemiluminescent flame intensity has been shown to decrease under circumstances where the flame temperature is increasing.

Instability and Extinction—Temperature field measurements allow for the assessment of and comparison between the magnitude of oscillation of the entire flame structure and that of the local flame front location (max T), as well as oscillation in peak temperature.

Sooty Flames—Measurements of the temperature field are needed to assess the local temperature at which soot is formed. Additionally, the maximum flame temperature for different ethylene concentrations can be assessed.

3.1.3.6 Far-Field Temperature Measurement

Six (6) locations are specified, with one at each orthogonal-component "of wall" and one at each orthogonal-component "of 10cm radius." Ambient temperature affects the flame temperature and hence extinction characteristics. 10cm radius corresponds to the "free area" performance volume specification.

Measurements of the ambient temperature near the chamber walls provide a requisite boundary condition for the problem and allow for the assessment of the growth of the flame structure. Concurrently, such measurements allows for the assessment of possible radiative heating of the chamber walls from the flame.

3.1.3.7 Radiant Emission

Global flame radiation needs to be measured in order to obtain the radiative heat loss from the entire flame. The spectral response should include CO_2 and OH* emission. Higher than video data acquisition rates are needed in order to capture oscillation phenomena. For measuring total flame emission as a function of time, a radiometer viewing the entire flame is envisioned. Radiative loss affects the flame temperature and hence extinction characteristics. Moreover, in order to perform an accurate energy balance it will be necessary to quantify heat transfer from the flame, requiring accurate measurements of the global flame radiation.

Flame Front Motion—Measurements of the radiative flux at a fixed position contribute to the assessment of the total thermal radiative loss rate, which should increase with the size of the flame structure. It is assumed that radiative heat loss from chemilluminescence is negligible.

Quasi-Steady Extinction—Measurements of the radiative flux at a fixed position will aid in determining the moment of extinction.

Instability and Extinction—Measurement of the radiative flux at a fixed position captures flame oscillations in the heat release rate, whose frequency and magnitude may be difficult to capture via direct imaging (i.e., cameras). Consequently, the rate of date acquisition for this diagnostic should be higher than that for direct imaging. The measured radiative flux will also be compared to directly imaged oscillations.

Sooty Flames—The radiative heat flux is expected to change at the onset of soot formation.

3.1.3.8 Post-Test Gas Composition (Desired)

The gas composition should be analyzed (e.g. with GC) locally near the wall at the end of an experiment. This will determine the validity of the imposed boundary condition. Additionally, the gases within the chamber should be well mixed and then analyzed to determine total oxygen consumption.

3.2 Operational Sequence

I. Establish chamber at constant pressure and species concentration.

II. Discharge fuel mixture through porous burner at the initial flow rate.

III. Ignite fuel mixture with hot wire coil and retract upon successful ignition.

IV. Allow for spherical diffusion flame to evolve.

V. Apply one of the following:

   a. Maintain flow rate with same initial mixture for duration of test (25s) or until extinction. See §5 for justification of this duration.

   b. Single step decrease in flow rate with same initial mixture at specified time, maintaining new flow rate for duration of test (25s) or until extinction.

VI. Terminate fuel supply to the burner after 25s.

The proposed flight experiment plan maximizes the value of a single test by satisfying multiple scientific objectives. The priority of the scientific objectives to be examined are ordered as listed in §2.1, for both non-sooty and sooty flames:

(**A**) Transient phenomenon leading toward steady flame

(**B**) Extinction phenomenon at “quasi-steady”-states

(**C**) Instability phenomenon, e.g. Le > 1 oscillations and Le < 1 wrinkling

By ignition with the flame not situated at the steady flame location, we will automatically observe (**A**). In studying (**B**), we may perhaps observe (**C**). So objectives (**A**), (**B**), and (**C**) may all be addressed by conducting a single experiment.

3.3 Test Matrix

REQUIRED

Exp Set	Sub Set	Fuel Mixture	Ambient	Flow rate (cc/s)	No. of runs
1	(a)	25%H_2/20%CH_4/55%**N_2**	21%O_2/79%**N_2**	(i) 5 (entire duration, 25s) (ii) 10 (entire duration, 25s) (iii) 15 (entire duration, 25s) (iv) 10 (5s)→2 (rest of duration) (v) 5 (5s)→2 (rest of duration)	5
	(b)	20%H_2/25%CH_4/55%**N_2**		(i) through (v) as shown above	5
	(c)	30%H_2/15%CH_4/55%**N_2**		(i) through (v) as shown above	5
	(d)	45%H_2/55%**N_2**		(x) 1 (entire duration, 25s) (y) 2 (entire duration, 25s) (z) 2 (5s)→0.5 (rest of duration)	3
	(e)	45%CH_4/55%**N_2**		(i) through (v) as shown in (a)	5
2	(a)	25%H_2/20%CH_4/55%**He**	21%O_2/79%**He**	(i) 5 (entire duration, 25s) (ii) 10 (entire duration, 25s) (iii) 15 (entire duration, 25s) (iv) 10 (5s)→2 (rest of duration) (v) 5 (5s)→2 (rest of duration)	5
	(b)	20%H_2/25%CH_4/55%**He**		(i) through (v) as shown above	5
	(c)	30%H_2/15%CH_4/55%**He**		(i) through (v) as shown above	5
	(d)	45%H_2/55%**He**		(x) 1 (entire duration, 25s) (y) 2 (entire duration, 25s) (z) 2 (5s)→0.5 (rest of duration)	3
	(e)	45%CH_4/55%**He**		(i) through (v) as shown in (a)	5
					Total: 46

HIGHLY DESIRED

Exp Set	Sub Set	Fuel Mixture	Ambient	Flow rate (cc/s)	No. of runs
3	(a)	20%C_2H_4/80%**N_2**	21%O_2/79%**N_2**	(i) 5 (entire duration, 25s) (ii) 10 (entire duration, 25s)	2
	(b)	25%C_2H_4/75%**N_2**		(i) and (ii) as shown above	2
	(c)	30%C_2H_4/70%**N_2**		(i) and (ii) as shown above	2
4	(a)	20%C_2H_4/80%**He**	21%O_2/79%**He**	(i) 5 (entire duration, 25s) (ii) 10 (entire duration, 25s)	2
	(b)	25%C_2H_4/75%**He**		(i) and (ii) as shown above	2
	(c)	30%C_2H_4/70%**He**		(i) and (ii) as shown above	2
					Total: 12

DESIRED

Exp Set	Sub Set	Fuel Mixture	Ambient	Flow rate (cc/s)	No. of runs
5	(a)	25%H_2/20%CH_4/55%$\mathbf{CO_2}$	21%O_2/79%$\mathbf{CO_2}$	(i) 5 (entire duration, 25s) (ii) 10 (entire duration, 25s) (iii) 15 (entire duration, 25s) (iv) 10 (5s)→2 (rest of duration) (v) 5 (5s)→2 (rest of duration)	5
	(b)	20%H_2/25%CH_4/55%$\mathbf{CO_2}$		(i) through (v) as shown above	5
	(c)	30%H_2/15%CH_4/55%$\mathbf{CO_2}$		(i) through (v) as shown above	5
	(d)	45%H_2/55%$\mathbf{CO_2}$		(x) 1 (entire duration, 25s) (y) 2 (entire duration, 25s) (z) 2 (5s)→0.5 (rest of duration)	3
	(e)	45%CH_4/55%$\mathbf{CO_2}$		(i) through (v) as shown in (a)	5
6	(a)	20%C_2H_4/80%$\mathbf{CO_2}$		(i) 5 (entire duration, 25s) (ii) 10 (entire duration, 25s)	2
	(b)	25%C_2H_4/75%$\mathbf{CO_2}$		(i) and (ii) as shown above	2
	(c)	30%C_2H_4/70%$\mathbf{CO_2}$		(i) and (ii) as shown above	2
					Total: 29

3.4 Test Matrix Summary

The test matrix (given above in §3.3) is designed to meet the complete success criteria, addressing all scientific objectives listed above.

All experimental sets will address transient phenomenon, as the flame evolves from localized ignition towards "steady" behavior, corresponding to Objective (**A**). The flames evolve in a quasi-steady state manner (becoming history independent), after a short initial transient. This issue is discussed in §Appendix 5.2.

The rationale for this test matrix is to utilize various mixtures to assess both chemical and transport effects (including radiative) on flame behavior. Pure H_2 and pure CH_4 are utilized to assess kinetic mechanisms associated with each. Additionally, pure H_2 only produces H_2O as its radiative product, thereby isolating its radiative properties. Mixtures composed of both H_2 and CH_4 are used to examine their combined chemical and transport effects. Various inerts which affect characteristic flame temperature and transport (molecular and radiative), all in the same mole fractions, are utilized for comparison. C_2H_4 allows for the examination of a fuel with nominal unity Le number. Additionally, its characteristic sooting nature directly addresses our basic science objectives focusing on (**A**) spreading of flame sheets, (**B**) dual extinction states, and (**C**) flamefront instabilities.

The fuel/inert mixtures in the REQUIRED experiment sets 1-2 include H_2/CH_4 mixtures (see subsets *a, b, c*) and H_2 and CH_4 as pure fuels (see subsets *d, e*) aimed at addressing chemical kinetic aspects. The inert mole fractions are all fixed at 55% for baseline comparison. As can be

seen, the difference between sets 1 and 2 is the inert (N_2 versus He), which is chosen to assess transport (e.g. diffusive properties) effects on flame stability. For example, experimental set 2 is aimed at inducing the pulsating instability for Le > 1, corresponding to Objective (**C**). The fuel components and their relative compositions are the same for sets 1-2, with different inert species in balance; similarly, the ambient composition reflects the use of a different inert species in the fuel mixture. It is noted that the characteristic flame temperatures (which will affect the Zeldovich number, Ze) will be different for the two experimental sets affecting stability and extinction.

Experiment sets 1-2 will also assess radiative extinction for high flow rates (see *i*, *ii*, *iii* under the flow rate category) and kinetic extinction for low flow rates (see *iv* and *v* under the flow rate category), corresponding to Objective (**B**). With regard to radiative extinction, mixture compositions of 25%H_2/20%CH_4, 20%H_2/25%CH_4, and 30%H_2/15%CH_4 have been shown in drop-tower experiments to be characterized by different radiative extinction times. These mixtures also eschew sooty ignition (due to strong H_2 presence), which can otherwise result in asymmetrically trapped soot that deteriorates flame sphericity. With respect to kinetic extinction, note that a step change from a higher flow rate to a lower one is needed because starting with a flow rate below the extinction limit would preclude flame establishment in the first place.

The HIGHLY DESIRED experiment sets 3-4 utilize C_2H_4 as fuel. With a nominal Le of unity with respect to air for this fuel, a baseline case (experiment set 3) for flame stretch and thermal-diffusive stability effects is established. The fuel and inert mole fractions for the C_2H_4/inert are varied to address different fuel concentration effects on sooting, which can impact Objectives (**A**) flame spread behavior, (**B**) extinction, and (**C**) flame stability. Soot will also enhance flame radiation. Since characteristic residence times will affect sooting tendencies, two flow rates are investigated for each mixture. Experiment set 4 replaces the inert, N_2, of set 3 with He, to better isolate Le>1 instabilities, corresponding to Objective (**C**), as well as examine extinction for characteristically higher flame temperatures.

The DESIRED experiment sets 5-6 examine the same fuel mixtures of the REQUIRED and HIGHLY DESIRED experiment sets, but with CO_2 as inert, including that for the ambient. N_2 and He are radiatively transparent gases; while CO_2 is an optically participating gas. While use of CO_2 should result in a characteristically lower flame temperature, the highly reabsorptive CO_2 species can minimize net radiative heat loss affecting flame dynamics and extinction. Objectives (**A**)-(**C**) are addressed by these experiments.

The maximum duration of any test is **25**s. See §5 for justification of this duration. A test is terminated early if the flame extinguishes.

3.5 Success Criteria

Success of the s-Flame Experiment will be judged on meeting the stated science objectives. Three different levels, minimal, substantial, and complete success, are defined below.

3.5.1 Minimal Success

Minimal success is defined to mean sufficient scientific data return from the experiment to perform a direct comparison with the numerical flame simulation and publish a single archival journal article. This minimal level of success may be achieved by obtaining (for example):

1. Observations of transient flame phenomena leading toward steady state flames for 1 CH_4 case and 1 C_2H_4 case. Such observations must include, at a minimum, the flow and boundary condition measurements, flame temperature data and image sequences from at least two orthogonal imaging systems; or
2. Observations of flame extinction at both low and high system Damkohler number for 1 case. Such observations must include, at a minimum, the flow and boundary condition measurements, flame temperature data and image sequences from at least two orthogonal imaging systems; or
3. Observations of spherical soot formation in 1 C_2H_4 case. Such observations must include, at a minimum, the flow and boundary condition measurements, flame temperature data and image sequences from at least two orthogonal imaging systems.

3.5.2 Significant Success

Significant Success is defined to mean sufficient scientific data return from the experiment to perform direct comparison with the numerical flame simulation resulting in multiple archival journal publications, but less return that defined for complete success. This significant level of success may be achieved by obtaining (for example):

1. Observations of at least two instances of flame front instabilities including at least one hydrocarbon fuel. Such observations must include, at a minimum, the flow and boundary condition measurements, and data quantifying the flame front oscillations from image sequences from at least two of the three imaging systems and from the radiometer instrument; or
2. Combinations or extensions (in terms of number of mixture ratios for a single hydrocarbon fuel or number of hydrocarbon fuels) of at least two of items 1 through 3 defined for minimum success; or

3.5.3 Complete Success

Complete Success is defined as meeting all of the experiment objectives, including as a minimum:

1. Observations of transient flame phenomena leading toward steady state flames for at least three different mixture ratios of each of two hydrocarbon fuels and two diluents. Such observations must include, at a minimum, the flow and boundary condition measurements, flame temperature data, image sequences from two orthogonal imaging systems, and radiometer data; and
2. Observations of flame extinction at both low and high system Damkohler number for at least three different mixture ratios of each of two hydrocarbon fuels and two diluents. Such observations must include, at a minimum, the flow and boundary

condition measurements, flame temperature data, image sequences from two orthogonal imaging systems, and radiometer data; and

3. Observations of at least two instances of flame front instabilities each including at least one hydrocarbon fuel. Such observations must include, at a minimum, the flow and boundary condition measurements, and data quantifying the flame front oscillations from image sequences from at least two orthogonal imaging systems and from the radiometer instrument; and
4. Observations of soot formation. Such observations must include the flow and boundary condition measurements, flame temperature data, image sequences from all imaging systems, temperature data, and radiometer data.

3.6 Post Flight Data Analysis Plan

Each test conducted on orbit will produce unique digital and imaging data – all of which are to be directly compared to the results of numerical simulations of the identical test conditions using the transient code developed under this program. These processed data sets are derived from the raw data produced by the experiment hardware, data acquisition, and imaging systems and conveyed to the investigator team through the flight hardware systems, space to ground communications systems, ground-based data handling systems, and the ground-based project operations team. These specific data sets are required to describe and evaluate the results of the flight experiments and to perform the comparisons between the experimental results and underlying detailed simulations of flames. In many instances, these data sets are required for analysis between successive test runs in order to either confirm or change the test conditions for the later tests. In each case, the data must be synchronized to a common time base that can be referenced to the ISS time standard. Except for the digital imaging data (i.e., items 2-4 and 6 below), the data must be provided to the investigator team in standard engineering units and in tabular electronic files such as a spreadsheet.

There are specific data sets that are needed:

1. **Flow and Boundary Conditions**, establishing the operating parameters of each test:
   a. **Burner flow rate and composition vs. time** for each test, derived from the monitoring data of one or more gas sources (fuel(s), diluent(s), oxygen). Establishes boundary conditions.
   b. **Ambient oxygen concentration vs. time**, derived from monitoring data obtained in the far field of the test chamber. Establishes boundary conditions.
   c. **Pressure vs. time**, derived from monitoring data obtained in the test chamber.
   d. **Three-axis accelerations vs. time**, derived from monitoring data obtained near the chamber. Establishes body forces imposed on flames.
   e. **Ambient temperature vs. time**, derived from monitoring data obtained in the far field of the test chamber. Establishes boundary conditions and heat loss rate to the far field.
   f. **Burner surface temperature vs. time**, derived from thermocouple or alternative measurements. Establishes flow boundary conditions and heat loss rate to the burner.

2. **Flame temperature vs. radius and time**, derived from imaging data by the PI's – e.g. thin filament pyrometry. Provides flame structure and the primary indication of flame extinction.

3. **UV intensity vs. radius and time**, related to emissions/concentrations of OH* and CH*, derived from digital images. Provides flame structure and one indicator of extinction.

4. **Visible Image vs. time**, derived from digital images. Provides visualization of flame behavior including symmetry, flame front velocities, extinction radius.

5. **Radiation flux vs. time**, derived from calibrated radiometer data. Provides estimate of total radiative flux from the flame and one indicator of flame extinction.

6. **Soot Volume Fraction vs Radius and Time**, derived from laser extinction measurements. Provides assessment of soot presence, especially that which may be at temperatures below the threshold for visible observation from incandescence.

Table 3.6 shows the relationship between these data sets and the Experiment Objectives. Data Sets 1, 2, and 5 are to be compared directly to the results of the numerical simulations. Image sequences 3 and 4 require complex processing including extraction of line intensity data along axi-symmetric chords, data inversion (Abel Transform) to obtain axi-symmetric distributions, conversion to relative species number density or temperature units.

Table 3.6 Data sets needed for analysis to support Science Objectives

Data Sets →	1. Flow and Boundary Conditions vs. Time	2. Flame Temperature vs. Radius and Time	3. UV Intensity vs. Radius and Time	4. Visible Image vs. Time	5. Radiation Flux vs. Time	6. Soot Volume Fraction vs Radius and Time
	Provides real-time independent variables and boundary conditions to which the flames respond	Provides transient and steady state flame structure, and…	Provides transient and steady state flame structure, and…	Visualization tool. Indicates flame symmetry and flame radius, and…	Estimates total radiative loss, and…	Provides soot concentration within the flame structure
↓ **Experiment Objectives**						
A. **Flame Front Motion**: Determine the transient flame structure of diffusion flames as they evolve and, in some instances, become steady state…	as above	Supports assessment of transport and chemical kinetics rates.	Supports assessment of chemical kinetics rates.	Used to compare flame and peak heat release rate locations.		**Indicates soot formation, which can be compared to visible emission of soot**
B. **Dual Extinction Limits at Low and High System Da**: Determine the quasi-steady convective/ chemical-kinetic and radiative/ chemical-kinetic extinction limits…	as above	Supports assessment of transport and chemical kinetics rates. Provides best indication of extinction.	Provides auxiliary indication of extinction.	(not a good indication of extinction)	Provides auxiliary indication of extinction.	**Indicates soot presence, which can be a source of radiative heat loss**
C. **Flame Front Instabilities in Non-Premixed Flames**: Demonstrate pulsating instabilities…	as above	as above	Shows dynamics of low frequency oscillations.	as above	Provides measure of pulsating flame front instability.	**Indicates soot presence, which can affect transport phenomena**

4.0 REFERENCES

Andrews, G.E., and Bradley, D., "Burning velocity of methane-air mixtures," *Combust. Flame* **18**:133-153 (1972).

Azzoni, R., Ratti, S., Aggarwal, S.K., Puri, I.K., "The structure of triple flames stabilized on a slot burner," *Combust. Flame* **119**(1-2):23-40 (1999).

Bennett, B.A.V., McEnally, C.S., Pfefferle, L.D., Smooke, M.D., and Colket, M.B.,, "Computational and experimental study of axisymmetric coflow partially premixed ethylene/air flames," Combust. Flame 127 (1-2):2004-2022 (2001).

Buckmaster, J., "Edge-flames," J. Eng. Math. **31**(2-3):269-284 (1997).

Buipham, M., and Seshardri, K., "Comparison between experimental measurements and numerical-calculations of the structure of heptane air diffusion flames," *Combust. Sci. Technol.* **79**(4-6):293-310 (1991).

Chao, B.H., Law, C.K., and T'ien, J.S., "Structure and extinction of diffusion flames with flame radiation," *Proc. Comb. Inst.* 23:523-531 (1990).

Cheatham, S., and Matalon, M., "Heat loss and Lewis number effects on the onset of oscillations in diffusion flames," *Proc. Comb. Inst.* **26**:1063-1070 (1996).

Christiansen, E. W., Sung, C. J., and Law, C. K., "Pulsating instability in near-limit propagation of rich hydrogen/air flames," *Proc. Comb. Inst.* **23**:555-562 (1998).

Christiansen, E.W., Tse, S.D., and Law, C.K., "A computational study of oscillatory extinction of spherical diffusion flames," submitted (2002).

Dietrich, D.L., Ross, H.D., and T'ien, J.S., "Candle flames in non-buoyant and weakly buoyant atmospheres," *AIAA 34th Aerospace Sciences Meeting*, AIAA-94-0429 (1994).

Hubbard, G. L., and Tien, C. L., "Infrared mean absorption coefficients of luminous flames and smoke," ASME J. Heat Transfer 100:235–239 (1978).

Joulin, G., and Clavin, P., "Linear stability analysis of nonadiabatic flames: diffusional-thermal model," *Combust. Flame* **35**:139-153 (1979).

Kent, J.H., and Williams, F.A., "Extinction of laminar diffusion flames for liquid fuels," *Proc. Comb. Inst* **15**:315-325 (1974).

King, M.K., "An unsteady-state analysis of porous sphere and droplet fuel combustion under microgravity conditions," *Proc. Comb. Inst*. **26**: 1227-1234 (1996).

Law, C.K., and Williams, F.A., "Kinetics and convection in the combustion of alkane droplets," *Combust. Flame* **19**:393-405 (1972).

Law, C.K., Chung, S.H., and Srinivasan, N., "Gas-phase quasi-steadiness and fuel vapor accumulation effects in droplet burning," *Combust. Flame* **38**:173-198 (1980).

Law, C.K., Li, T.X., Chung, S.H., Kim, J.S., and Zhu, D.L., "On the structure and extinction dynamics of partially-premixed flames: theory and experiment," *Combust. Sci. Technol.* **64**:199-232 (1989).

Lee, J., and Chung, S.H., "Characteristics of reattachment and blowout of laminar lifted flames in partially premixed propane jets," Combust Flame **127**(4):2194-2204 (2001).

Liñán, A., "The asymptotic structure of counterflow diffusion flames for large activation energies," *Acta Astronautica* **1**:1007-1039 (1974).

Lozinski, D., and Matalon M., "Combustion of a spinning fuel droplet," *Combust. Sci. Technol.* **96**:345-367 (1994).

Mills K., and Matalon, M., "Burner-generated spherical diffusion flames," *Combust. Sci. Technol.* **129**(1-6):295-319 (1997).

Nayagam, V., Haggard, J.B., Colantonio, R.O., Marchese, A.J., Dryer, F.L., Zhang, B.L., Williams, F.A., "Microgravity n-heptane droplet combustion in oxygen-helium mixtures at atmospheric pressure," *AIAA J.* **36**(8):1369-1378 (1998).

Okai, K., Moriue, O., Araki, M., Tsue, M., Kono, M., Sato, J., Dietrich, D.L., Williams, F.A., "Pressure effects on combustion of methanol and methanol/dodecanol single droplets and droplet pairs in microgravity," *Combust. Flame* **121**(3):501-512 (2000).

Pearlman, H.G., and Sohrab, S.H., "Diffusion flame extinction and viscous hydrodynamics around rotating porous spheres with surface blowing," *Combust. Flame* **108**:419-441 (1997).

Peters, N., *Turbulent Combustion*, Cambridge University Press, 2000.

Puri, I.K., and Seshardri, K., "The extinction of counterflow premixed flames burning diluted methane-air, and diluted propane-air mixtures," *Comb. Sci. Tech.* **53**(1):55-65 (1987).

Puri, I.K., Aggarwal S.K., Ratti S., et al., "On the similitude between lifted and burner-stabilized triple flames: a numerical and experimental investigation," *Combust. Flame* **124**(1-2):311-325 (2001).

Sivashinsky, G.I., "Diffusional-thermal theory of cellular flames," *Combust. Sci. Technol.* **15**:137-146 (1977).

Sivashinsky, G.I., "Instabilities, pattern formation, and turbulence in flames," *Ann. Rev. Fluid Mech.* **15**:179-199 (1983).

Tien, C. L., Advances in Heat Transfer, "Thermal radiation properties of gases," New York: Academic Press, Vol. 5, pp. 253–324 (1968).

Tien, J.S., "Diffusion flame extinction at small stretch rates: the mechanism of radiative loss," *Combust. Flame* **65**:31-34 (1986).

Tse, S.D., Zhu, D.L., and Law, C.K., "Morphology and Burning Rates of Expanding Spherical Flames in H_2/O_2/Inert Mixtures up to 60 Atmospheres," *Proc. Comb. Inst.* **28**: 1793-1800 (2000).

Tse, S.D., Zhu, D., Sung, C.J., Ju, Y., and Law, C.K., "Microgravity Burner-Generated Spherical Diffusion Flames: Experiment and Computation," *Combust. Flame* **125**:1265-1278 (2001).

Wu, C.K., and Law, C.K., "On the determination of laminar flame speeds from stretched flames," *Proc. Comb. Inst.* **20**:1941-1949 (1985).

Yoo, S.W., Law, C.K., and Tse, S.D., "Chemiluminescent OH* and CH* flame structure and aerodynamic scaling of weakly buoyant, nearly spherical diffusion flames," *Proc. Comb. Inst.* **29**, in press.

5.0 APPENDICES

5.1 Oxygen Replenishment Considerations

A spherical combustion chamber with a radius of 28.794cm (100L) is assumed. The temperature at the wall is fixed at 300K. A fuel mixture of 20%H_2-25%CH_4-55%N_2 at a fixed mass flow rate of 0.01572g/s is issued through 0.635cm radius burner. This flow rate is large for a "worst case scenario." The flame is ignited a few millimeters away from the burner surface.

Figure A.1 shows the pressure increase in the chamber, as well as the depletion of oxygen at a radius of 20cm (corresponding to the radius of the CIR chamber), for an *adiabatic* flame expanding outwardly in a constant volume chamber. By 200s, the chamber pressure has almost doubled, and by 50s, oxygen depletion is already noticeable.

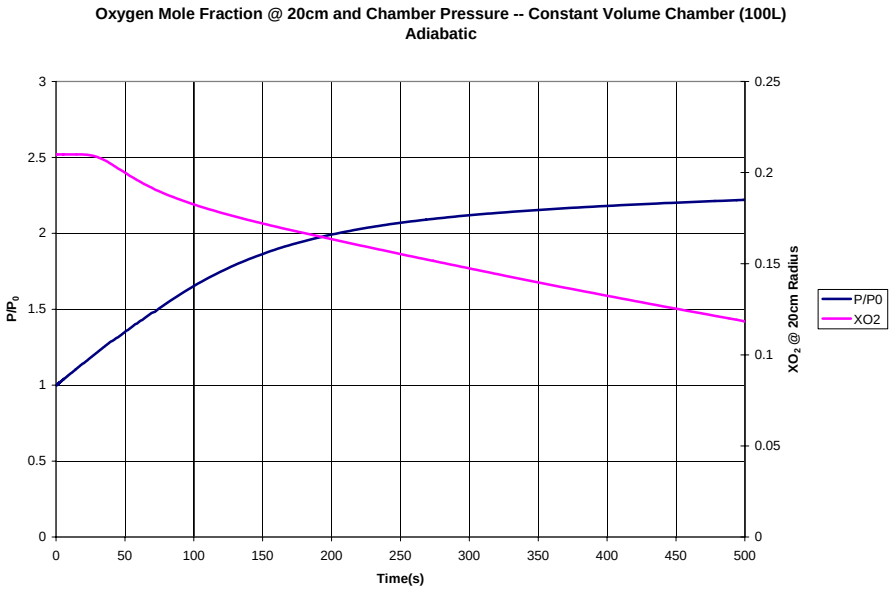

Figure A.1.

Figure A.2(a) shows the corresponding oxygen mole fraction profiles for different times. The "penetration depth" for oxygen reaches r=20cm at t=25s, for the constant volume case. Figure A.2(b) shows the constant pressure case for comparison, where oxygen depletion starts to occur at r=20cm at t=20s.

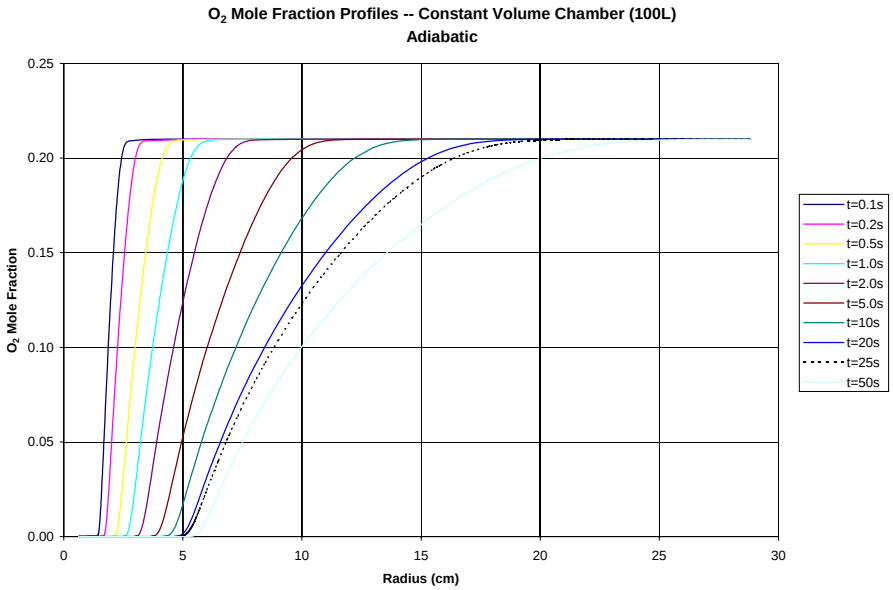

Figure A.2(a)

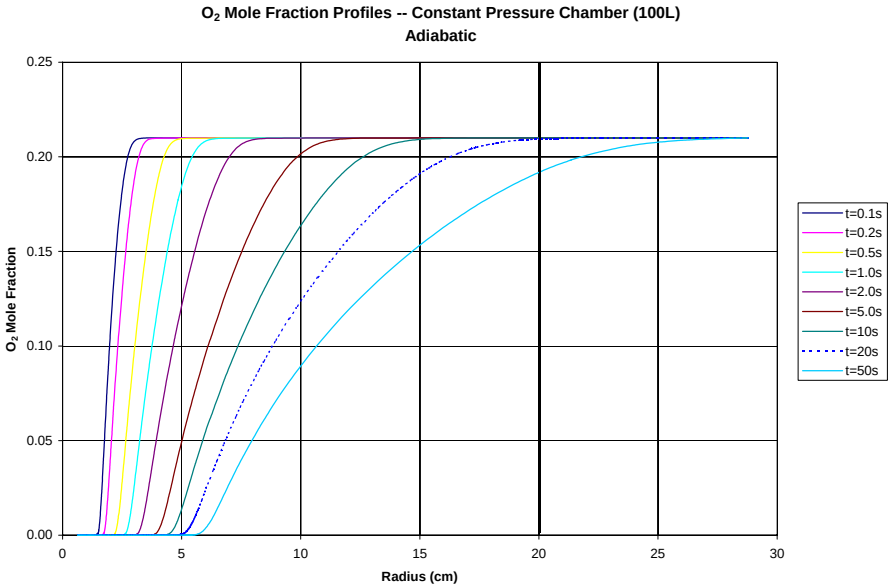

Figure A.2(b)

Figure A.3 shows the temperature profiles for different times, comparing the constant volume and constant pressure cases. The "penetration depths" of the temperature profiles follow those of the oxygen profiles. The temperatures of the constant volume case are slightly higher than for the constant pressure case.

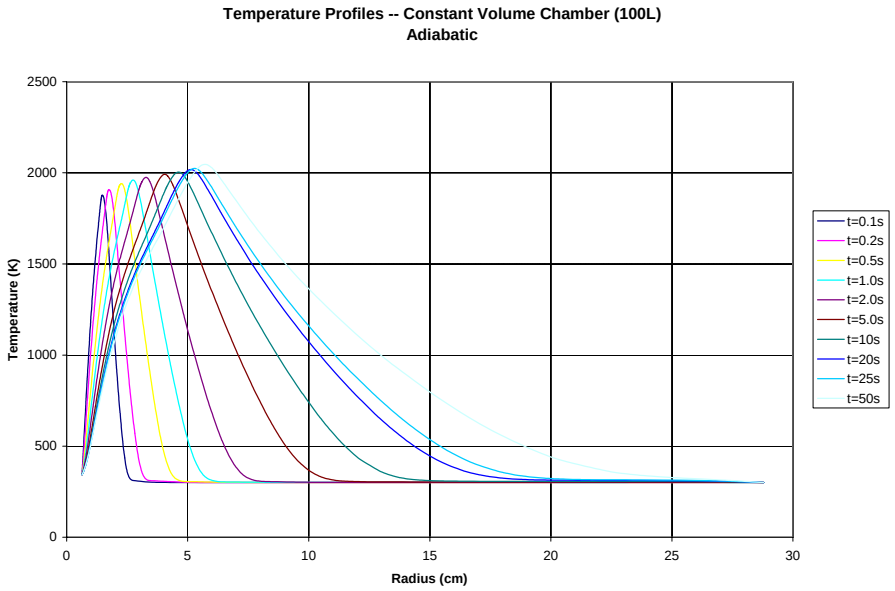

Figure A.3(a)

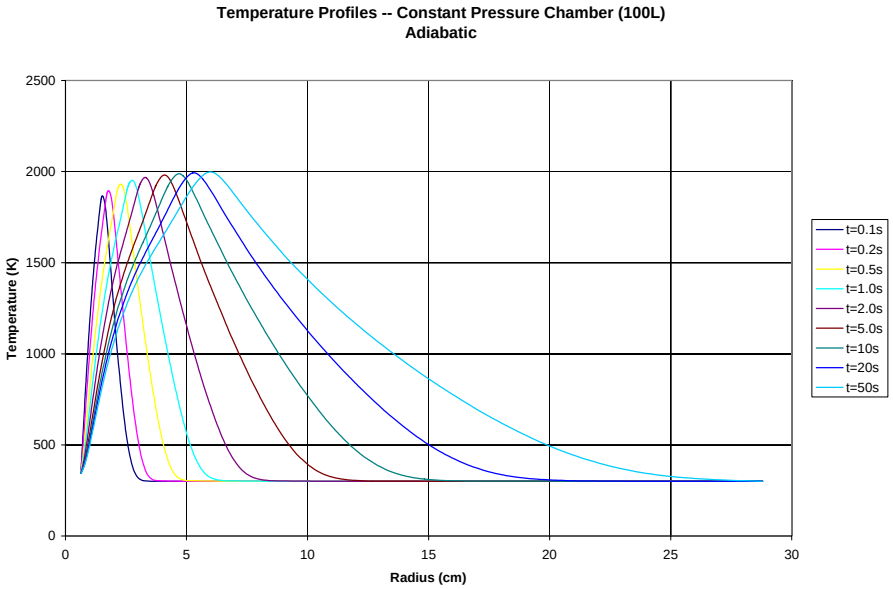

Figure A.3(b)

Figure A.4 compares the flame position (for Max Temperature) for the constant volume and constant pressure cases. As expected, the constant volume flame grows slower compared to the constant pressure. This is because the flame radius is a function of the mass flow rate at the flame. Although the mass flow rate at the burner is fixed, the mass flow distribution in space is vastly different between the constant volume and constant pressure cases.

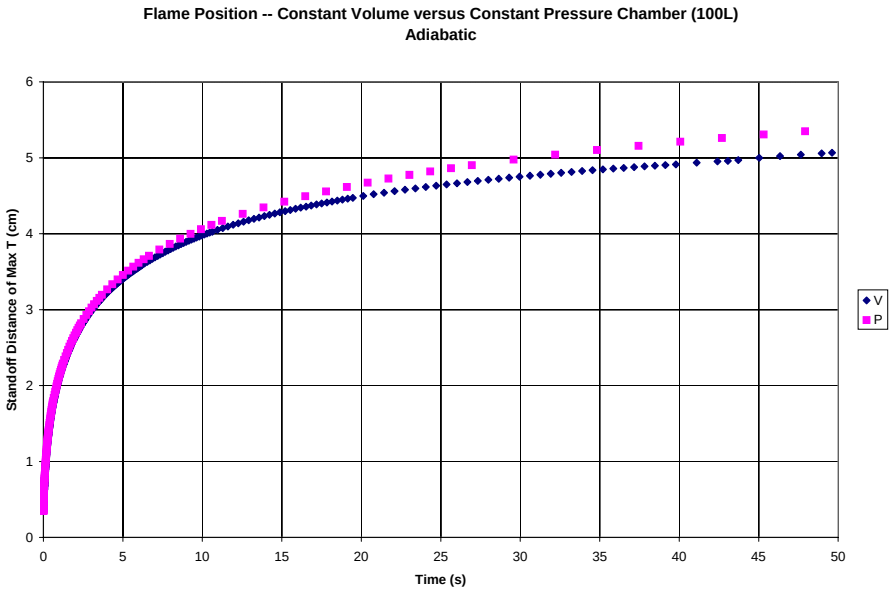

Figure A.4.

Figure A.5 compares the constant volume and constant pressure cases for the flames including radiative loss with gas-phase reabsorption. The constant volume flame is seen to extinguish slightly later than the constant pressure flame.

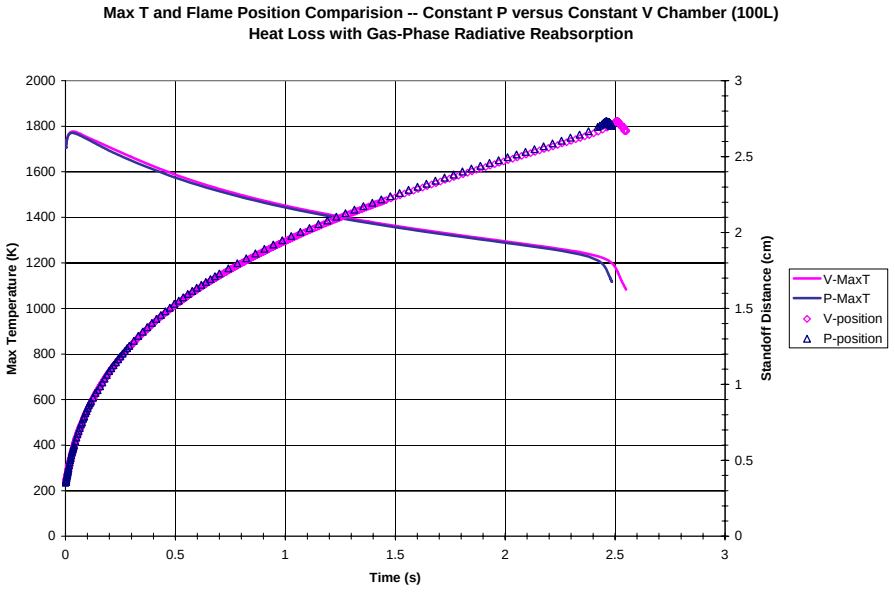

Figure A.5.

5.2 Quasi-Steady Flame Movement

The quasi-steady conservation equations, in the reference frame moving with the reaction front, for mass, energy, and species are given by:

$$\frac{\partial \dot{m}}{\partial x} + 2\frac{A}{r}\rho U_f = 0, \tag{A.a}$$

$$\dot{m}\frac{\partial T}{\partial x} - \frac{1}{c_p}\frac{\partial}{\partial x}\left(A\lambda\frac{\partial T}{\partial x}\right) + \frac{A}{c_p}\sum_{k=1}^{K}\rho Y_k V_k c_{p_k}\frac{\partial T}{\partial x} + \frac{A}{c_p}\sum_{k=1}^{K}\dot{\omega}_k h_k W_k = 0 \tag{A.b}$$

$$\dot{m}\frac{\partial Y_k}{\partial x} + \frac{\partial}{\partial x}\left(\rho A Y_k V_k\right) - A\dot{\omega}_k W_k = 0\,, \tag{A.c}$$

where

$$\dot{m} \equiv \rho(u - U_f)A\,,\ A \equiv 4\pi r^2\,,\ \mathrm{d}x \equiv \mathrm{d}r - U_f\,\mathrm{d}t\,. \tag{A.d}$$

U_f is the moving velocity of the flamefront.

The flamefront location, assumed to correspond to that of peak temperature, can be solved for, within the framework of gas-phase quasi-steadiness in the flame coordinate, as a function of flamefront velocity. For an evolution problem, the flamefront position and its velocity are related by $U_f \equiv \mathrm{d}r_f/\mathrm{d}t$. Thus, for a given initial flamefront position, the trajectory of the flamefront can be completely determined.

Within the framework of gas-phase quasi-steadiness, the flamefront motion process can be described as follows. Since the flame is initially situated close to the porous burner and far from the steady-state flame position, the fuel mass consumption rate at the flame is smaller than the fuel production rate from the burner. Consequently, the flamefront spreads outwardly, as it seeks the steady-state position where the fuel consumption and fuel production rates are equal, resulting in an accumulation of the fuel vapor between the droplet surface and flame. It is the flamefront motion itself, adjusting its velocity in order to completely consume the mass flow of fuel entering its reaction zone that governs the quasi-steady expansion behavior.

5.3 Heat Transfer to Burner Considerations

To attempt to address the worst-case scenario, we examine the adiabatic case (at constant pressure) with no radiative loss. Note that the burner represents only the solid material and not the gas inside it. Ideally, the burner should be adiabatic such that all of the heat conducted toward it from the flame is directly transferred to the gas mixture within it, with its only purpose being to provide a uniform flow field. Consequently, the entire flow-field temperature distribution including an adiabatic burner should be the same as that for a point source issuing fuel mixture at zero radius. Here, we assume that the initial mixture temperature is 300K. Figure A.6 compares the *initial* temperature profiles (where a flame is ignited a few millimeters away from the burner surface) for an adiabatic case and one where the temperature at the burner surface is measured to be 350K (20%H_2-25%CH_4-55%N_2, 15.72 mg/s).

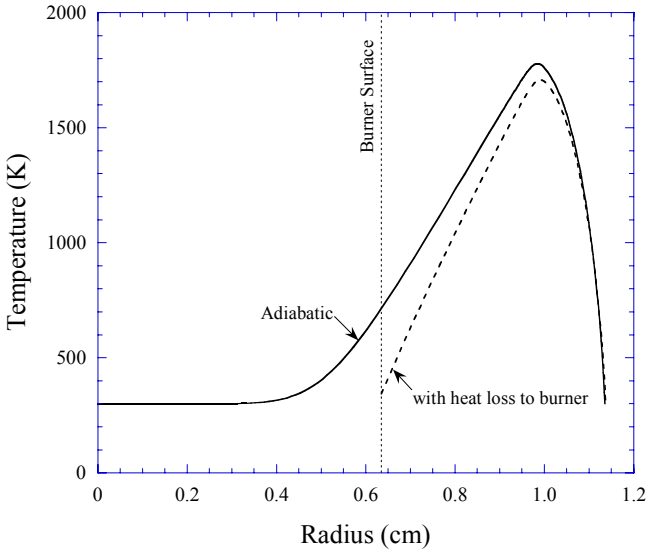

Figure A.6.

Obviously, the flame temperature is reduced due to heat loss to the burner. What is interesting, though, is that for the adiabatic case, the temperature gradient is minimal up to 0.4cm from zero radius. Thus if the burner were 0.3175cm (0.5 × 0.635cm) in radius, then, for the same mixtures and mass flow rates, heat loss to the burner would be negligible. Nonetheless, the effect of heat loss to the burner on flame properties such as trajectory and Max T is small for the transient evolution of the case of Fig. A.6, as shown in Fig. A.7.

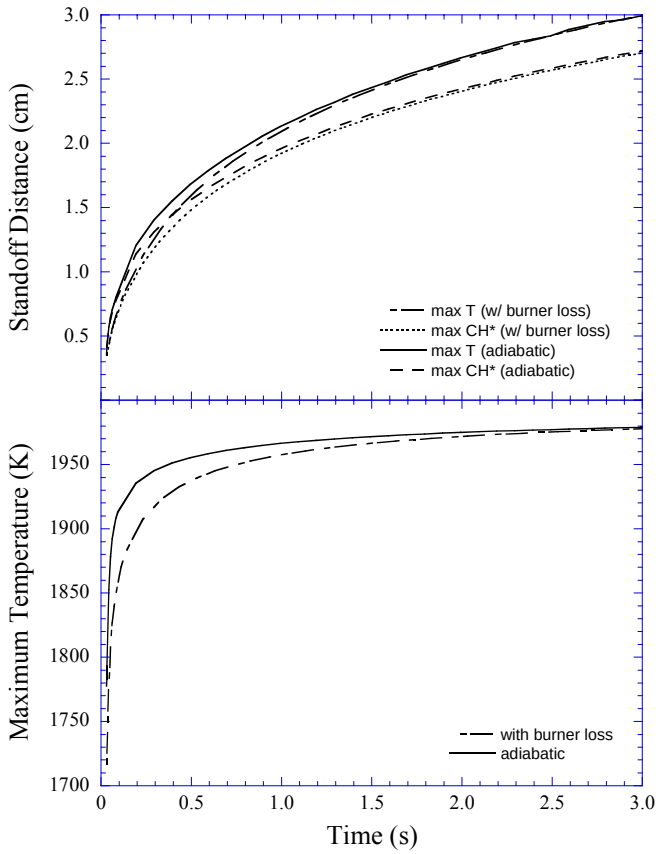

Figure A.7.

As a result, the primary concern is the performance of the burner at high temperatures. The highest temperatures are reached under adiabatic conditions. Figures A.8 and A.9 show the transient evolution of the burner surface temperature for a 0.3175cm radius burner, for different mixtures and mass flow rates.

The adiabatic "burner" temperature reaches the highest temperature for the lowest mass flow rates. However, as can be seen, the maximum burner temperatures are less than 400C. Moreover, inevitable heat loss to the burner will result in a even lower temperature. Consequently, it seems that burner overheating should not be a problem.

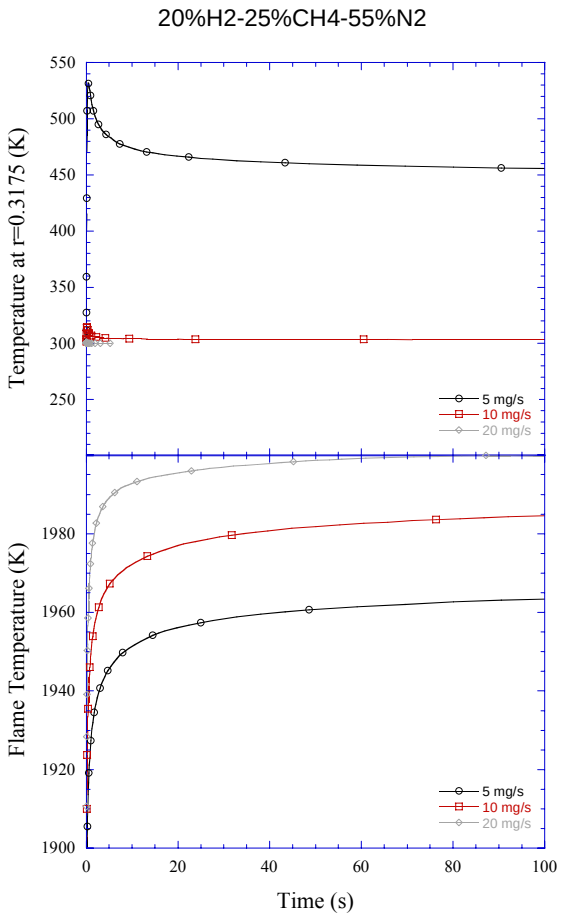

Figure A.8

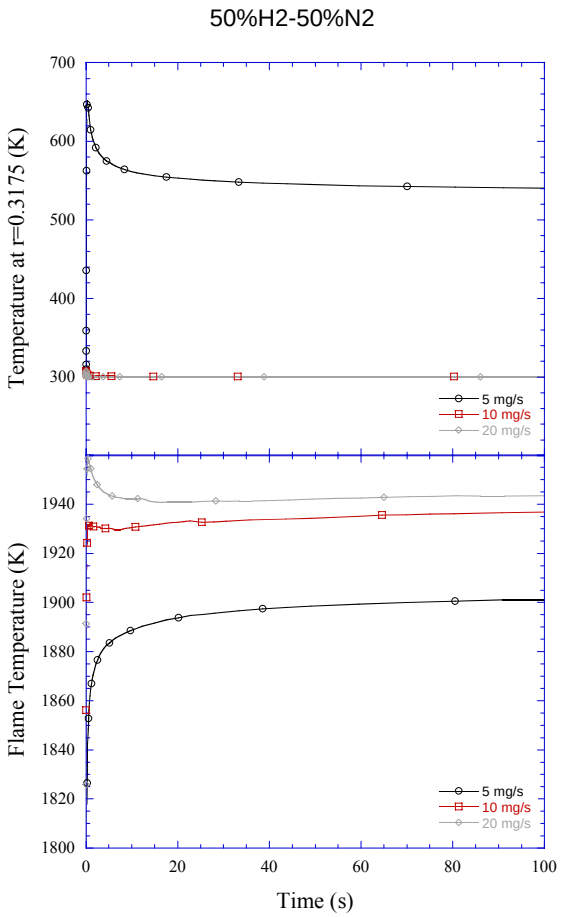

Figure A.9

5.4 UV Imaging: Comparison with Experiment and Computation

A nearly-spherical, "inverse" hydrogen flame was formed by issuing a 9%O_2/91%N_2 mixture of mass flow rate m = 0.078 g/s into a pure hydrogen environment at a chamber pressure of 0.079 atm. A chemiluminescence image of electronically-excited hydroxyl radical was captured by a Xybion IMC-201 intensified multispectral video camera with a 50-mm, UV-transmissive lens and narrowband interference filter centered at 310nm with full-width, half maximum of 20nm. Flame luminosity was always contained within the focal depth of the camera system, so that the image could be treated as a line-of-sight projection. After digital image filtering and processing, the 2-D projections were spatially deconvoluted (separately for half of the "symmetric" projections) to map local luminosity as a function of radial position. A "3-dimensional" images of the flame chemiluminescence were then constructed from vertical stacks of Abel deconvoluted two-dimensional slices. Figure A.10(a) shows the OH* flame projection image, and Fig. A.10(b) shows the Abel deconvoluted image.

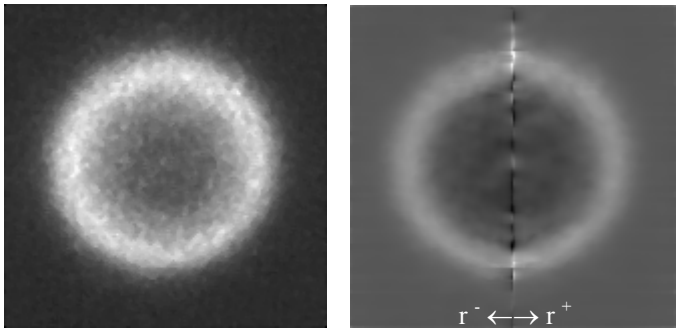

(a) (b)

Figure A.10

The experimental flame was computationally simulated using the Sandia burner-stabilized premixed flame code, with boundary conditions modified for nonpremixed burning. The mass flow rate, burner surface temperature, and ambient temperature were specified by the experiment, along with the boundary mixture compositions. Additionally, the computational domain size was set so that the computed maximum temperature location corresponded to that measured experimentally. As it turned out, the resulting computational domain size equaled the effective spherical radius (24.8cm), calculated from the physical volume of the non-spherical chamber.

The reaction mechanism used was based on the $H_2/O_2/N_2$ mechanism developed by Mueller [1], which consists of 9 species and 21 elementary reaction steps, obtained at conditions ranging from 0.3 to 15.7atm and 850–1040K. OH* chemiluminescence reactions were added to the above mechanism. OH* in the first electronically excited state is produced primarily from the reaction H + O + M → OH* + M. At the same time OH* disappears by the quenching step OH* + M → OH + M and by photon emission OH* → OH + hν, corresponding to the transition $^2\Sigma^+ \rightarrow {}^2\Pi$, observable at 305.4nm. The rate constants for these steps were taken from Refs. [2, 3], with the heat of formation for OH* set at 93kcal/mol above that of ground-state OH.

Figure A.11 shows the computational prediction of the flame structure. The arrow indicates the location of the measured maximum temperature.

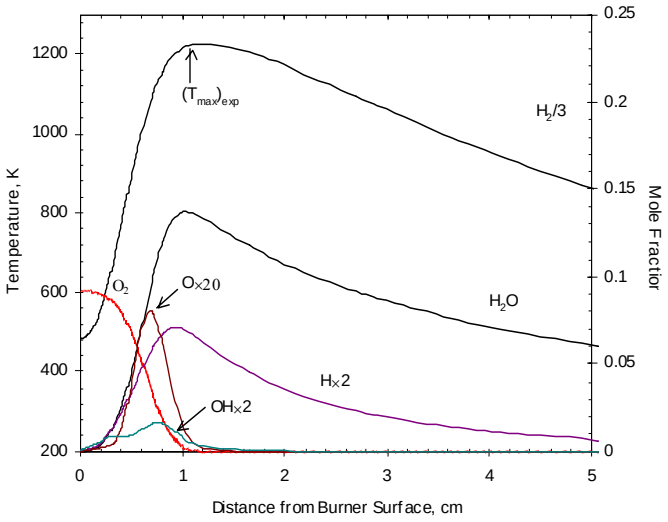

Figure A.11.

The experimental and computational OH* intensity profiles, normalized by their respective maximum values, are shown in Fig. A.12.

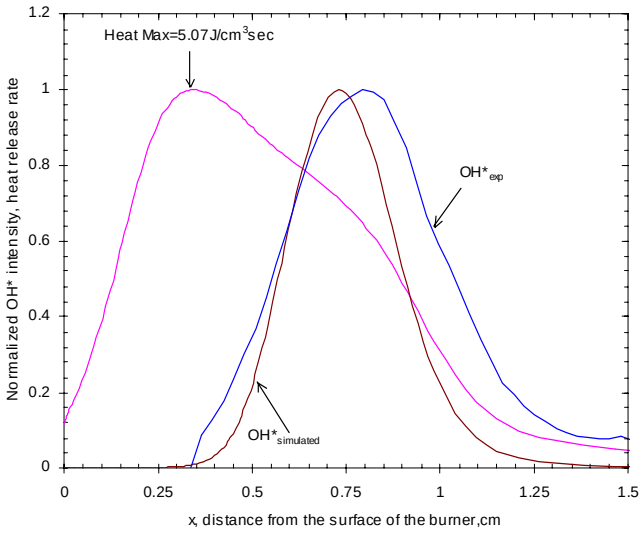

Figure A.12.

The experimentally measured OH* profile is a bit wider than the computational one, with the peak slightly shifted by 0.06 cm away from the flame. Nonetheless, the comparison is very favorable, suggesting not only that the degree of spherical symmetry for the flame is high, but also that such experimental measurements of the flame structure can be quantitatively valid.

It should be noted that our technique of spatially resolving 3D distribution of OH* have been limited to identifying peak locations for flame front tracking. Quantification of the absolute radical concentration by calibrating the chemiluminescence intensity to the images is currently underway.

References

1. Mueller, M. A., Kim, T. J., Yetter, R. A., and Dryer, F. L., *Int. J. Chem. Kinet*., 31: 113-125 (1999).
2. Hidaka, Y., Takahashi, S., Kawano, H., Suga, M., and Gardiner, W. C., *J. Phys. Chem*., 86: 1429-1433 (1982).
3. Dandy, D. S., and Vosen, S. R., *Combust. Sci. and Tech*., 82: 131-150 (1992).

5.5 *g*-Jitter Considerations

EFFECTS OF ACCELERATION ENVIRONMENT ON THE STABILITY OF SPHERICAL DIFFUSION FLAMES (S-FLAME)

Douglas Feikema, Project Scientist
NASA Glenn Research Center
Microgravity Combustion Science
Cleveland, OH 44135

PI: C.K. Law, Princeton University

CO-I's: S.D Tse, Rutgers Univ. and

Kurt Sacksteder, NASA Glenn

Poster Paper at 2nd Joint Meeting of the Combustion Institute, Oakland, CA March, 2001

INTRODUCTION

OBJECTIVE:

• Analyze effect of KC-135 free float environment on the stability of spherical diffusion flames to evaluate Quasi-steady, Vibratory, and Transient-Impulsive Acceleration Limits

• Compare results with the ISS Design Requirement

APPROACH:

• Analyze synchronized, time-resolved, Video and acceleration vectors

• Two Free Float KC-135 Parabola's Discussed

• 8.0 second clean free-float parabola to study vibratory limit

• 3.5 second event to study a transient-impulsive event

G-jitter Levels in Various Facilities with One-Third Octave Bands

Reference: Ross, 2001, Microgravity Combustion: Fire in Free Fall

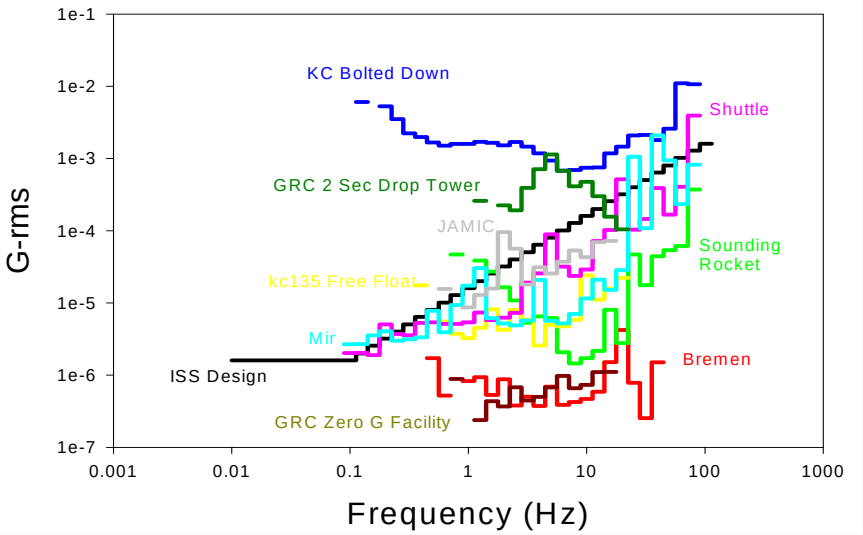

ISS Design Requirement Acceleration Environment

The design requirement acceleration environment on ISS with ARIS (vibration isolation system) as presently projected. (NASA SSP 410000 Version E)

1. The duration of the microgravity environment will be for 180 days per year in continuous time intervals of at least 30 days.
2. The quasi-steady acceleration (< 0.01 Hertz) will have magnitude less than or equal to 1 micro-g. Also, the component perpendicular to the orbital average acceleration vector will be less than or equal to 0.2 micro-g.
3. The transient acceleration limit for individual disturbance sources is less than or equal to 1000 micro-g per axis and the integrated transient acceleration limit is less than or equal to 10 micro-g seconds per axis over any 10 second interval.
4. The vibratory acceleration limit is $0.01 \le f \le 0.1$ Hertz; $g_{RMS} \le 1.6$ µg; $0.1 \le f \le 100$ Hertz; $g_{RMS} \le f \times 16$ µg; $100 \le f \le 300$ Hertz; $g_{RMS} \le 1600$ µg. where f is frequency and g_{RMS} is the root-mean-square acceleration magnitude.

S-Flame Insert on GIFFTS Rig

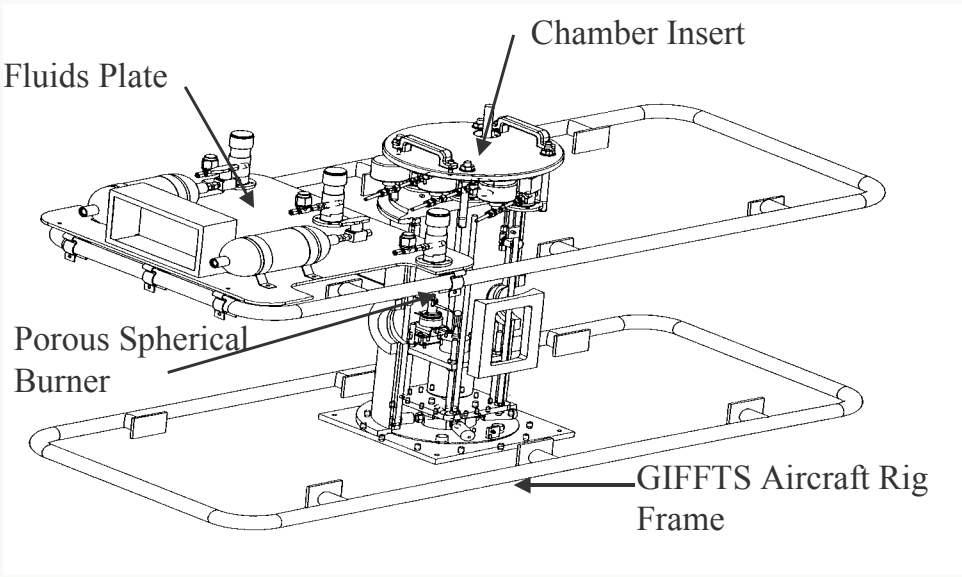

8.0 seconds of "Clean" Free Float 3-D Acceleration and Power Spectrum on KC-135 to Study Vibratory Limit

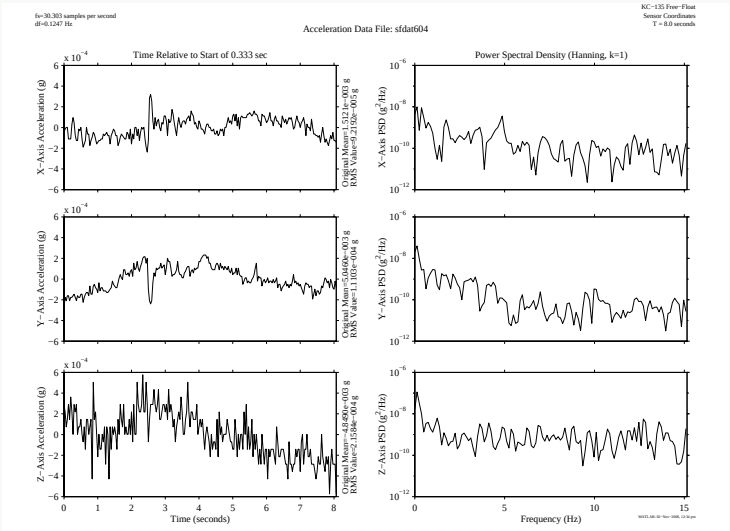

X-Axis: For/Aft ; Y-Axis: Wing to Wing; Z-Axis: Up/Down
Signals have been Demeaned

One Third Octave Band Comparison of 8 sec "Clean" KC-135 Parabola with ISS Design

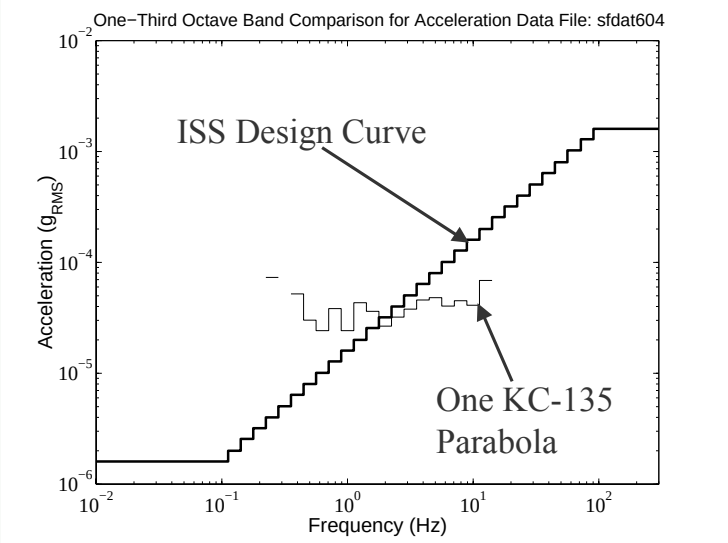

Video Clips of False Colored "Blue" Flames for 8 second "Clean" Free Float Parabola

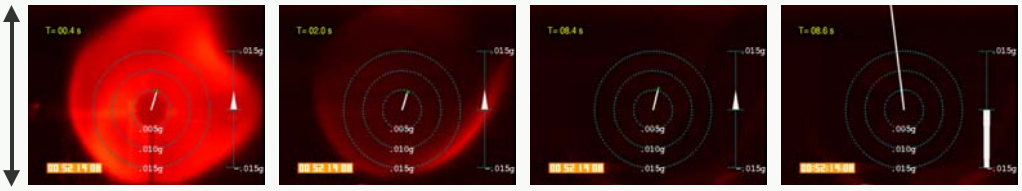

11.4 cm

Figure 3 (a) t = 0.4 sec

Figure 3 (b) t = 2.0 sec

Figure 3 (c) t = 8.4 sec

Figure 3 (d) t = 8.6 sec

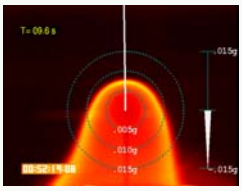

Figure 3 (e) t = 9.0 sec

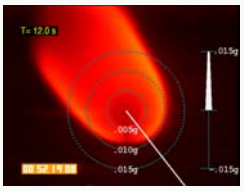

Figure 3 (f) t = 9.3 sec

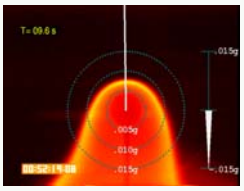

Figure 3 (g) t = 9.6 sec

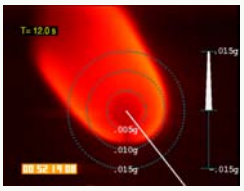

Figure 3 (h) t = 12.0 sec

Fuel: 20%H2/25% CH4/ 55% N2 @ 22.6 mg/sec in Ambient Dry Air

Impulsively Disturbed Free Float Parabola: Acceleration and Power Spectrum on KC-135: 3.5 seconds

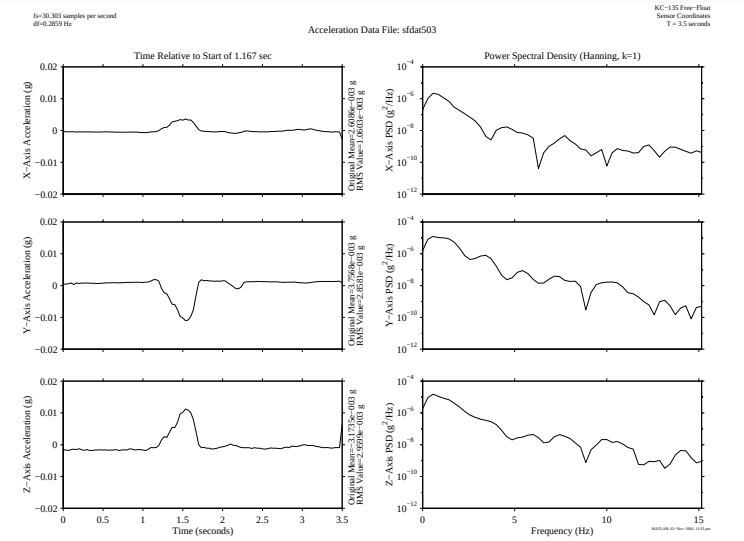

X-Axis: For/Aft ; Y-Axis: Wing to Wing; Z-Axis: Up/Down
Signals have been Demeaned

One Third Octave Band Comparison of Impulsively Disturbed 3.5 sec KC-135 Parabola with ISS Design

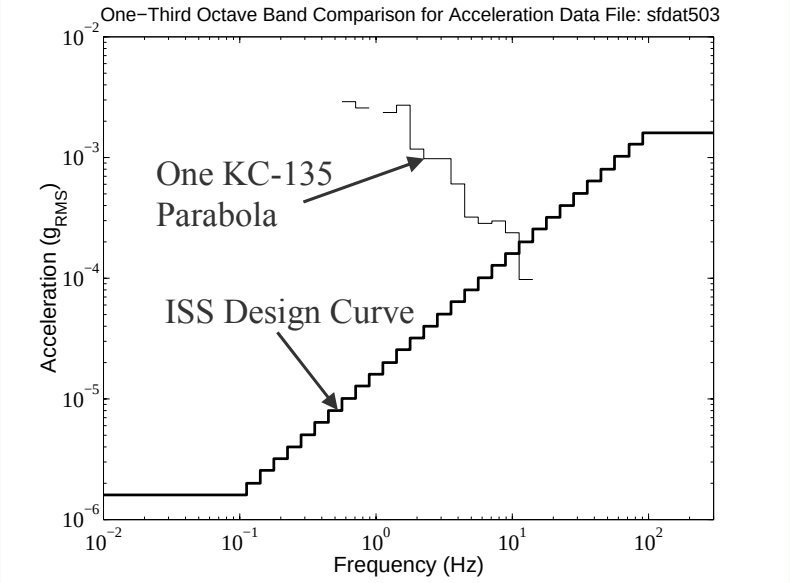

Video Clips of False Colored "Blue" Flames for Free Float Parabola with Impulsive Disturbance

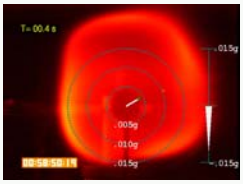

Figure 6(a) t = 0.4 seconds

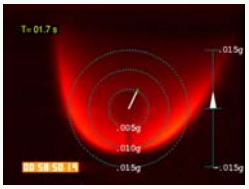

Figure 6(b) t = 1.7 seconds

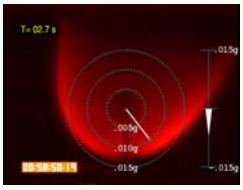

Figure 6(c) t = 2.7 seconds

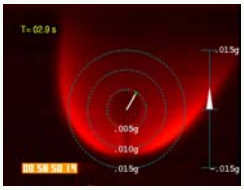

Figure 6(d) t = 2.9 seconds

12 cm

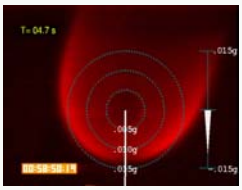

Figure 6(e) t = 4.6 seconds

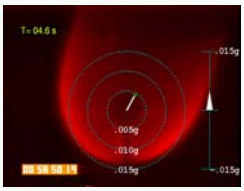

Figure 6(f) t = 4.7 seconds

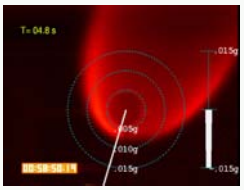

Figure 6(g) t = 4.8 seconds

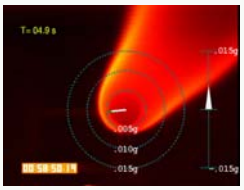

Figure 6(h) t = 4.9 seconds

Fuel: 20%H2/25% CH4/ 55% N2 @ 19.7 mg/sec in Ambient Dry Air

Estimates of Threshold Acceleration Levels from Grashof and Richardson Numbers

Grashof Number: $$Gr = \frac{\beta \Delta T g L^3}{\nu^2} \propto \frac{\text{Buoyant Forces}}{\text{Viscous Forces}}$$

For $Gr_{Critical} = 0.1$ $g_{Threshold} = 1.4 \times 10^{-7}\ g_E$

For $Gr_{Critical} = 1.0$ $g_{Threshold} = 1.4 \times 10^{-6}\ g_E$

Richardson Number: $$Ri = \frac{gL}{U^2} \propto \frac{\text{Buoyant Forces}}{\text{Momentum or Inertial Forces}}$$

For $Ri_{Critical} = 0.1$ $g_{Threshold} = 4 \times 10^{-5}\ g_E$

For $Ri_{Critical} = 1.0$ $g_{Threshold} = 1.4 \times 10^{-4}\ g_E$

Experiment: $5 \times 10^{-3}\ g_E$ disturbs "large" spherical diffusion flames

S-Flame Acceleration Requirement

1. Quasi-steady: $0.01 \leq f \leq 0.1$ Hertz; $g \leq 5.0$ μg per axis
2. Vibratory: ISS Design with ARIS Acceptable
3. Transient-Impulsive: $\leq$ 25 μg-seconds per axis over any 5 second interval

Conclusions

1. For g-jitter greater than threshold levels, the buoyant portion of flame aligns itself with g-vector but in opposing direction, Time Lag for alignment process on the order of 1 second.
2. ISS design vibratory limits sufficient for spherical diffusion flames
3. Integrated transient-impulsive disturbance of magnitude 2500 micro-g-seconds (10,000 micro-g disturbance of duration 0.5 seconds) disturbs flame. ISS design considered acceptable for transient-impulsive disturbances
4. Difficult to generate "large" spherical diffusion flames even in free float on parabolic aircraft due to milli-g type aerodynamic drag manifested as residual acceleration. Similar flames in 2.2 second drop tower are much more spherical.
5. Smaller Spherical Diffusion Flames more stable since threshold acceleration levels higher as predicted by scaling laws.